

This is a repository copy of *Contemporary Salt-Marsh Foraminifera from Southern California and Implications for Reconstructing Late Holocene Sea-Level Changes*.

White Rose Research Online URL for this paper:

<https://eprints.whiterose.ac.uk/198974/>

Version: Published Version

---

**Article:**

Avnaim-Katav, Simona, Garrett, Ed, Gehrels, Willem Roland et al. (5 more authors) (2023) Contemporary Salt-Marsh Foraminifera from Southern California and Implications for Reconstructing Late Holocene Sea-Level Changes. *Journal of Foraminiferal Research*. pp. 157-176. ISSN 0096-1191

<https://doi.org/10.2113/gsjfr.53.2.157>

---

**Reuse**

This article is distributed under the terms of the Creative Commons Attribution (CC BY) licence. This licence allows you to distribute, remix, tweak, and build upon the work, even commercially, as long as you credit the authors for the original work. More information and the full terms of the licence here:

<https://creativecommons.org/licenses/>

**Takedown**

If you consider content in White Rose Research Online to be in breach of UK law, please notify us by emailing [eprints@whiterose.ac.uk](mailto:eprints@whiterose.ac.uk) including the URL of the record and the reason for the withdrawal request.

# CONTEMPORARY SALT-MARSH FORAMINIFERA FROM SOUTHERN CALIFORNIA AND IMPLICATIONS FOR RECONSTRUCTING LATE HOLOCENE SEA-LEVEL CHANGES

SIMONA AVNAIM-KATAV<sup>1,\*</sup>, ED GARRETT<sup>2</sup>, W. ROLAND GEHRELS<sup>2</sup>, LAUREN N. BROWN<sup>3</sup>, THOMAS K. ROCKWELL<sup>4</sup>, ALEXANDER R. SIMMS<sup>5</sup>, JOHN MICHAEL BENTZ<sup>5</sup> AND GLEN M. MACDONALD<sup>3,6</sup>

## ABSTRACT

**We report on the distribution of contemporary foraminifera in salt marshes in Mission Bay and Carpinteria Slough, Southern California. Combining these data with existing datasets from Seal Beach and Tijuana, we explore the potential for a regional training set to underpin quantitative reconstructions of paleoenvironmental change from foraminifera preserved in salt-marsh sediments. We demonstrate that species' distributions are highly dependent on elevation, suggesting fossil foraminiferal assemblages here, as in many other regions, are useful depositional elevation indicators. Transfer functions provide predictions from Mission Bay cores with decimeter-scale uncertainties. Nevertheless, interpretation of marsh-surface elevation change is complicated by a complex geomorphic setting and anthropogenic impacts. An abrupt change in elevation in the mid-1700s may be related to lateral spreading of water-saturated sediments during an earthquake on the Rose Canyon fault, suggesting the potential for foraminifera to support new palaeoseismic and sea-level records for the region.**

## INTRODUCTION

Studies of sediment successions from salt marshes provide opportunities for quantitative reconstructions of late Holocene relative sea- and land-level changes around the world (Guilbault et al., 1996; Gehrels et al., 2004; Sawai et al., 2004; Kemp et al., 2011). Quantitative sea-level studies rely on modern faunal or floral zonation with respect to elevation over a range generally covering the intertidal zone and occasionally extending into subtidal environments (e.g., Horton et al., 1999; Gehrels et al., 2001; Woodroffe, 2009; Avnaim-Katav et al., 2016). Once the relationship between the relative abundance of different species of a particular microfossil group and elevation is established, it is used to develop predictive transfer functions capable of inferring the past elevation relative to the tidal frame from fossil records (Barlow et al., 2013; Kemp & Telford, 2015). Within

salt-marsh sedimentary archives, benthic foraminifera are among the most commonly used microorganisms for reconstructing past sea-level changes due to their vertical zonation in the modern intertidal zone (e.g., Scott & Medioli, 1980; Scott et al., 1984; Gehrels, 1994; Horton et al., 1999; Kemp et al., 2009; Horton & Edwards, 2005). They work particularly well in micro- to mesotidal settings (Barlow et al., 2013; Kemp & Telford, 2015; Williams et al., 2021). With sufficient sampling resolution, transfer functions can provide a near-continuous record of sea-level change with precision of ~0.1–0.3 m (Williams et al., 2021).

Microfossil transfer functions are widely applied to reconstruct the direction and magnitude of abrupt coseismic changes in land level, which are experienced along coastlines as sudden changes in relative sea level (Hocking et al., 2017; Shennan et al., 2016; Brader et al., 2021). The Newport–Inglewood–Rose Canyon fault zone is a large and active fault system that extends along ~70 km of the southern California coast (Sahakian et al., 2017). Substantial vertical deformation may not be expected along this strike-slip fault system; nevertheless, intense shaking may still result in marsh submergence and abrupt relative sea-level rise due to lateral spreading and sediment consolidation (Aydan et al., 2008). Consequently, in areas subject to these processes, relative sea-level rise results in an increase in accommodation space, leading to distinct and observable changes in paleoecological records (Darienzo & Peterson, 1995; Nelson et al., 1996; Shennan et al., 2016). Such submergence of coastal salt marshes might be evident in the abrupt transition from a peaty soil to intertidal mud deposition, as shown in numerous studies exploring earthquakes along the Cascadia Subduction Zone (e.g., Darienzo & Peterson, 1995; Nelson et al., 1996; Shennan et al., 1996; Atwater & Hemphill-Haley, 1997).

In Southern California, Avnaim-Katav et al. (2017) developed a transfer function using a modern foraminiferal training set from two salt marshes. However, the range of elevations covered by this training set was limited, and no comparison with fossil foraminiferal assemblages was undertaken. Consequently, this study first aims to create a robust and extensive regional-scale modern training set from which transfer functions can be developed. To achieve this we describe the distribution of contemporary foraminiferal assemblages with regards to elevation in two southern Californian salt marshes, Kendall-Frost Mission Bay Marsh Reserve and Carpinteria Slough, before merging them with the data of Avnaim-Katav et al. (2017). Secondly, we seek to test the applicability of the resulting transfer functions by investigating fossil foraminiferal assemblages from three cores from the Kendall-Frost Mission Bay Marsh Reserve near San Diego. We use quantitative reconstructions of changes in relative sea level to discuss initial interpretations of the

<sup>1</sup> Israel Oceanographic & Limnological Research Haifa 3108001, Israel

<sup>2</sup> Department of Environment and Geography, University of York, Heslington, York, YO10 5NG, United Kingdom

<sup>3</sup> University of California, Los Angeles, Department of Geography, 1255 Bunche Hall, Box 951524, Los Angeles, CA 90095, USA

<sup>4</sup> Department of Geological Sciences, San Diego State University, MC-1020, 5500 Campanile Dr., San Diego, CA 92182-1020, USA

<sup>5</sup> Department of Earth Science, University of California Santa Barbara, Santa Barbara, CA 93111, USA

<sup>6</sup> University of California, Los Angeles, Institute of the Environment and Sustainability, La Kretz Hall, Suite 300, Box 951496, Los Angeles, CA 90095-1496, USA

\* Correspondence author. E-mail: simonaav@ocean.org.il

sea-level, tectonic, and anthropogenic history of the site and identify directions for future palaeoseismic and relative sea-level research along this populous coastline.

## STUDY AREA

### KENDALL-FROST MISSION BAY MARSH RESERVE

Kendall-Frost Mission Bay Marsh Reserve is located in northern Mission Bay (32°47'N, 117°13'W; Fig. 1). This salt marsh occupies 6.5 ha of the 16-ha total of wetlands that comprise the Northern Wildlife Preserve maintained by the City of San Diego. Around the time of Spanish settlement (1769 CE), Mission Bay, or Puerto Falso, named by the Spanish due to its large estuarine entrance which they falsely thought to be San Diego Bay, was a deep-water embayment surrounded largely by marsh and mudflat habitat (Fig. 1). Rerouting the San Diego River's course into Mission Bay in 1850, followed by enhanced siltation turned it into a shallow embayment. Intense dredging and rerouting of the river through a flood control channel were part of developing Mission Bay into a small-craft harbor and recreation area during the 1940s, preserving two remnant marshes, Kendall-Frost marsh reserve and Famosa Slough (Marcus, 1989).

Studies on foraminiferal ecology in Mission Bay date back to the 1960s and mid-late 1970s. Phleger & Bradshaw (1966) discussed the low species richness within intertidal environments compared to subtidal environments, associated with rapid changes in their abiotic parameters over a tidal cycle. Scott (1976) studied the recent paleoecology of this and other southern Californian salt marshes. Scott et al. (2011) integrated these earlier results with borehole sediments aimed to reconstruct Holocene paleoenvironmental changes; however, cores were collected close to an old river channel that may have biased the stratigraphic record.

Pristine, unaltered salt marshes suitable for sea-level reconstruction are lacking along the southern Californian coastline. Human activity has greatly reduced the extent of salt-marsh environments and caused substantial geomorphic changes, as detailed above. Nevertheless, through the application of palaeoenvironmental reconstruction approaches, it may be possible to disentangle the anthropogenic impacts and other processes including long-term sea-level change and abrupt changes associated with earthquakes. Such abrupt changes associated with coseismic deformation or intense shaking are anticipated given the close proximity of the site to the Newport–Inglewood–Rose Canyon fault zone, a large and active strike-slip fault system (Fig. 1). The fault zone is part of the broad, distributed shear zone comprising the Pacific–North American plate boundary. Most long-term slip in Southern California occurs on the San Andreas, San Jacinto, and Elsinore faults but 12–15% of the ~50 mm/yr of plate boundary shear is attributed to the coastal and offshore faults, including the Newport–Inglewood–Rose Canyon fault zone (Sahakian et al., 2017).

### CARPINTERIA SLOUGH

Carpinteria Slough (34°24.0'N, 119°31.5'W) lies approximately 15 km east of Santa Barbara and 150 km northwest of the Seal Beach site investigated by Avanim-Katav et al. (2017) (Fig. 1). The 230-ha marsh consists of three basins;

the two eastern basins are separated from the western basin by an artificial road. Channels within the eastern half of the marsh are channelized and dredged, resulting in a highly altered tidal flushing of the marsh plain (Sadro et al., 2007). The western basin contains a much more complex array of tidal channels and creeks, which are largely unaltered (Sadro et al., 2007); therefore, we focused our surface sampling on this area. Tidal input and drainage primarily occurs through a tidal inlet, which sits at the southern margin of the marsh (Sadro et al., 2007). The marsh is separated from the open Santa Barbara Channel by a spit that has been breached during large multi-century storms (Reynolds et al., 2018).

## TIDES, VEGETATION, AND CLIMATE

Mission Bay and Carpinteria Slough share similar climatic and oceanographic settings, representative of Southern California. Tides along the open coast are semidiurnal and have a mean range of ~1.2 m. We discuss site-specific tidal ranges in the 'METHODS' section.

The marshes demonstrate a vegetation zonation typical of the marshes of Southern California (Zedler, 1977; Zedler et al., 1986). The lowest vegetated zone is characterized by *Spartina alterniflora*. The mid-marsh zone is commonly co-dominated by *Sarcocornia pacifica*, *Batis maritima*, and *Jaumea carnosa*. *Distichlis spicata*, *Frankenia grandifolia*, and *Limonium californicum* occur in the mid-to-high marsh areas. The boundary between mid and high marsh vegetation is less well-defined, and plants from these zones also inhabit the marsh-upland transition area. *Arthrocnemum subterminale* and *Monanthochloe littoralis* prefer the highest marsh elevations. The marsh-upland transition is marked by the presence of shrub-type plants, such as *Artemisia californica*, *Rhus lauriana*, and *Baccharis pilularis*.

The climate of Southern California is Mediterranean (Xeric) and characterized by hot, dry summers and cool to warm, wet winters. The average annual high and low temperatures are 21°C and 14.1°C, and the annual precipitation average is 26.4 cm (usclimatedata.com). Drought and extreme flooding are common and pose substantial climatic impacts on marsh vegetation (Zedler et al., 1986; Zedler, 2010; Reynolds et al., 2018). During the dry season (March to September) marsh soils are characteristically hypersaline because most of the soil moisture originates from tidal inundation and because evaporation typically exceeds precipitation (Zedler, 1982).

## METHODS

### MODERN SAMPLE COLLECTION AND PREPARATION

To assess the distribution of tidal-marsh foraminifera we collected 11 surface samples from Mission Bay and 29 from Carpinteria Slough. At both sites, we established a linear sampling transect (Fig. 1; Appendix 1). At Carpinteria Slough, this was supplemented by an additional broad swath of samples (17 in total, prefaced CS\_ES; Fig. 1). Sampling at Mission Bay incorporated low, mid, and high marsh vegetation zones, with samples from Carpinteria Slough also extending down into the upper part of the unvegetated tidal flat. Sampling along transects (e.g., within one site/marsh)

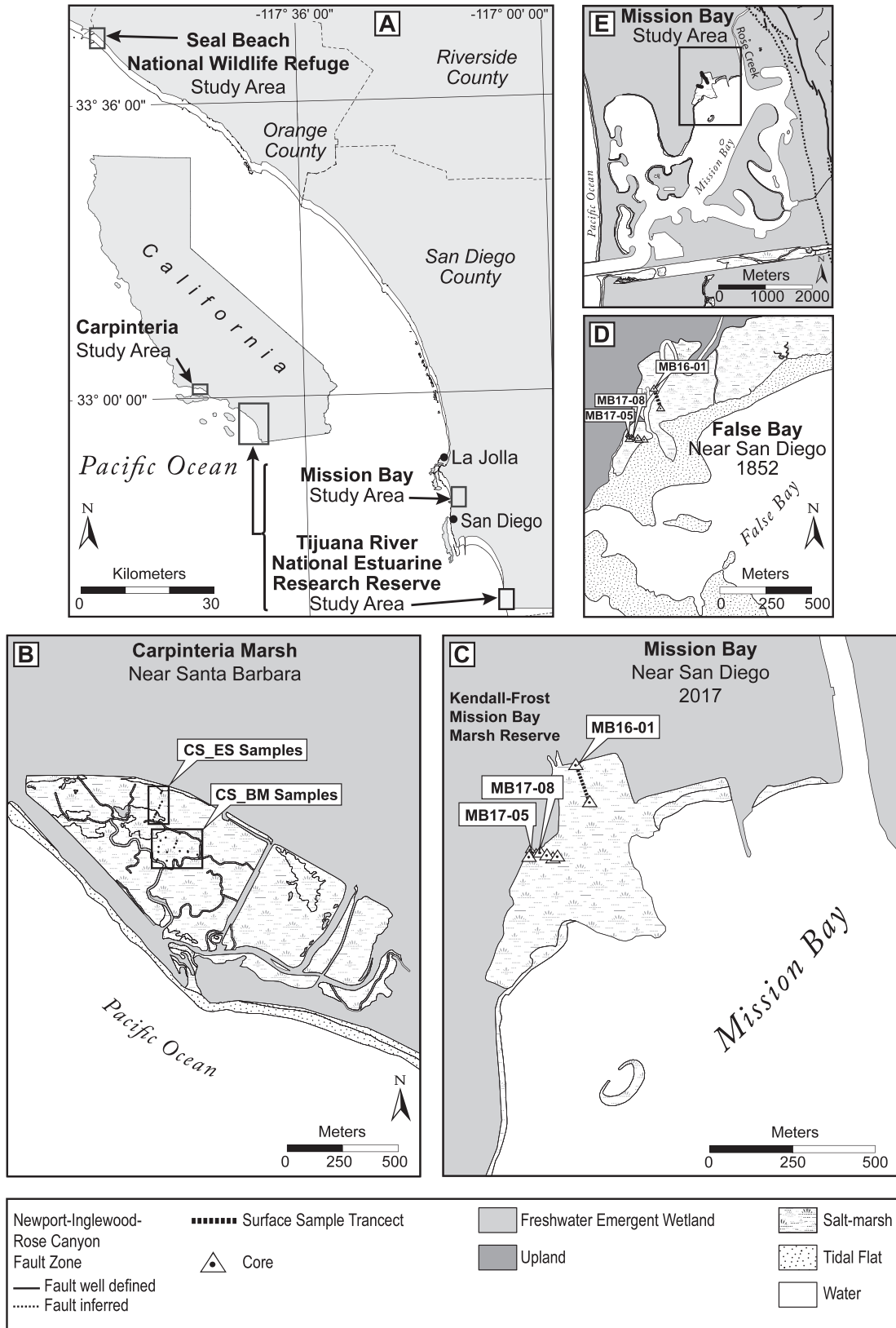


FIGURE 1. Location of the study area on the Southern California coast including the sites studied in Avnaim-Katav et al. (2017) and new sites explored in this study (A), including Carpinteria Slough (B), and Mission Bay salt marsh (C), with transects highlighted showing the surface station (dots) and core (triangles) locations. Cores analyzed in this study are specified also in the 1852 historic map (D) and in the geologic map of the San Diego (E). Coordinates of surface sample and core locations are available in Appendices 1 and 2.

may lead to spatial autocorrelation and thus might negatively affect transfer function model performance (Legendre & Fortin, 1989; Telford & Birks, 2009). The issue of spatial autocorrelation is reduced by including samples from different salt marshes and combining the results into one modern training set. To this end, we combine the 40 samples reported in this paper with 51 modern surface samples reported by Avnaim-Katav et al. (2017) from marshes in the Seal Beach and Tijuana estuaries (Fig. 1).

At each surface sampling location, we sampled a standardized volume of 10 cm<sup>3</sup> from the topmost centimeter of salt-marsh sediment (10 cm<sup>2</sup> by 1 cm thick) for foraminiferal analysis. This sampling strategy has been widely used in many marshes studied around the world, although it does not capture the presence of infaunal species (Scott & Medioli, 1980; Patterson et al., 2004). Sample preparation followed Schönfeld et al. (2012) and Avnaim-Katav et al. (2017). Samples were stained with rose Bengal solution (2 g rose Bengal/1 95% ethanol) at the time of sampling. Rose Bengal confirms the presence of cytoplasm and is widely used to distinguish between dead and assumed living foraminifera. As cytoplasm may potentially persist for years or decades after death (Bernhard et al., 2006), “live” counts may also include recently living foraminifera. Nevertheless, comparing rose Bengal with the vital stain CellTracker Green, Figueira et al. (2012) suggested no significant difference between the ability of the two staining techniques to discriminate between live and dead foraminifera in tidal marsh samples. Specimens were included in an “assumed living at the time of collection” category when multiple chambers were stained bright red (Horton & Edwards, 2006; Milker et al., 2015). The solution was buffered by calcium carbonate powder to avert dissolution of calcareous species. Samples were wet sieved through 500- $\mu$ m and 63- $\mu$ m sieves. The >500- $\mu$ m fraction was analyzed for larger foraminifera before being discarded. The fraction between 63 and 500  $\mu$ m was subdivided into eight equal aliquots using a wet splitter (Scott & Hermelin, 1993).

Tests were counted in water, which enabled easy detection of rose Bengal-stained foraminifera in the surface samples and prevented drying of the organic residue. Samples with more than 50 dead tests were used in numerical analyses, following Kemp et al. (2020). Two samples from Carpinteria Slough were excluded from the analysis due to low counts. Consequently, eighty-nine samples were included in the modern training set.

Taxonomic identifications follow the World Foraminifera Database (Hayward et al., 2022). Juvenile specimens of Trochamminids were lumped into a single group because they were difficult to identify to species level due to their small sizes but excluded from statistical analyses as they reflect a range of species that inhabit different elevations. All counts were expressed as a relative abundance (%). Scanning electron microscope photographs of key species were taken at the Department of Earth, Planetary and Space Sciences, UCLA.

#### LEVELLING AND TIDAL DATA

The locations of the surface samples were determined with a Differential Global Positioning System (dGPS). Each lo-

cation was post-processed with the Online Positioning User Service produced by the US National Oceanic and Atmospheric Administration (NOAA) to standardize and correct for spatial changes in mean sea level, MSL. The elevations, with a precision averaging 4 cm, were referenced to the North American vertical datum (NAVD88) computed using GEOID12B.

Following Avnaim-Katav et al. (2017), we use NOAA’s vDatum tool (<http://vdatum.noaa.gov/>) to assess tidal datums [mean higher high water (MHHW), mean tide level (MTL), and mean lower low water (MLLW)] at Mission Bay salt marsh (Table 1). While vDatum provides datums for the open coastline, the enclosed nature of Mission Bay could result in modification of the tidal amplitude. Nevertheless, NOAA predictions for Quivira Basin, within Mission Bay and around 3 km south of the sampled marsh, suggest no tidal dampening occurs (NOAA, 2022).

For Carpinteria Slough, we use datums derived by Sadro et al. (2007) from a vented pressure sensor deployed between August 2005 and April 2006 (Table 1). While Avnaim-Katav et al. (2017) used vDatum to derive tidal datums for Tijuana, we update their analysis using five years of data from the National Estuarine Research Reserve System (<http://cdmo.baruch.sc.edu/dges/>). We use water-level data from Oneonta Slough for the period from September 2016 to August 2021 to define MTL and MHHW (Table 1). This reanalysis results in a smaller tidal range than used in the previous publication.

We convert the elevation of each modern sample to a standardized water level index (SWLI), which allows us to combine samples from sites with different tidal ranges into a single training set (Gehrels, 1999; Barlow et al., 2013; Kemp & Telford, 2015). Wright et al. (2011) recommend using the highest occurrence of foraminifera as the upper reference level in SWLI calculations. However, we could not establish this datum because our highest samples still contained foraminifera. Consequently, we used MHHW as the upper reference level. Our index assigns MHHW at each site a SWLI value of 200 and MTL a value of 100.

We assume that the tidal range in Mission Bay has not changed over time. Natural and anthropogenic modification of Mission Bay means that this assumption may not be accurate; however, we do not have any data to support the use of alternative tidal ranges when converting SWLI values back into meters. The consequence of this is that rates of past changes may be overestimated or underestimated. In particular, for abrupt changes in relative sea level, the magnitude of the change may be miscalculated. Consequently, all such estimates should be viewed as initial approximations and potentially subject to later recalculation if new evidence for tidal range changes arises.

#### STATISTICAL ANALYSIS

Dead surface foraminiferal assemblages, rather than total or live assemblages, were statistically analyzed to minimize the influence of seasonal fluctuations (Culver & Horton, 2005; Milker et al., 2015). While the living assemblage represents a single point in time and may be influenced by seasonal blooms, dead assemblages provide time-averaged information about the assemblages, and thus most accurately

TABLE 1. Tidal datums for each study site including Mean Higher High Water (MHHW), Mean Tide Level (MTL), and Mean Lower Low Water (MLLW). Datums for Carpinteria are from Sadro et al. (2007); those from Tijuana are based on five years of tidal data from publicly available water level data (<http://cdmo.baruch.sc.edu/dges/>). Datums for Mission Bay and Seal Beach are generated using the National Oceanic and Atmospheric Administration (NOAA) vDatum tool.

Site	Latitude	Longitude	MHHW (m NAVD88)	MTL (m NAVD88)	MLLW (m NAVD88)	Great diurnal tidal range (m)
Kendall-Frost Mission Bay Marsh	32.7931	-117.2306	1.60	0.79	-0.08	1.68
Tijuana River Estuary	32.5706	-117.1321	1.63	1.16	0.75	0.88
Seal Beach	33.7402	-118.0861	1.59	0.80	-0.06	1.66
Carpinteria Marsh	34.3997	-119.5385	1.64	1.06	0.63	1.01

reflect the subsurface assemblages. The following statistical methods were applied to the combined foraminiferal and elevation data from four salt marshes: Mission Bay, Carpinteria Slough, Tijuana, and Seal Beach.

In order to classify the distribution of groups and subgroups in the foraminiferal samples into homogeneous faunal zones (clusters) we used a Q-mode cluster analysis in PRIMER version 6 software (Clarke & Gorley, 2006) following steps described in Avnaim-Katav et al. (2017). Rare species (<1 % maximum relative abundance) were excluded from the analysis.

A detrended canonical correspondence analysis (DCCA; Ter Braak, 1986) was carried out to determine the type of response, unimodal or linear, displayed by the species to the elevation gradient. With gradient lengths ('species turnover') of >2 standard deviation units, our DCCA indicated a unimodal species response and therefore canonical correspondence analysis (CCA) was applied to quantify the relationship between the distributions of benthic foraminifera and elevation. Both DCCA and CCA were applied using Canoco, version 4.55 software (ter Braak & Šmilauer, 2002; Lepš & Šmilauer, 2003) following the steps detailed in Avnaim-Katav et al. (2017).

The relationship between elevation (SWLI) and the relative abundances of foraminiferal taxa was empirically modelled using transfer functions. We do not apply any species transformation or remove any outlying samples. Transfer functions were developed using Weighted Averaging (WA; ter Braak, 1987), Weighted Averaging Partial Least Squares (WAPLS; ter Braak & Juggins, 1993) and Locally Weighted Averaging (LWWA; Juggins & Birks, 2012) in C2 version 1.7.4 (Juggins, 2011). For LWWA we include 30 samples in the "local" training set and use the chord-squared distance metric. Transfer function performance was evaluated based on widely applied criteria (Birks, 1998; Juggins & Birks, 2012; Kemp & Telford, 2015). The model with the highest bootstrapped  $r^2$  (1000 cycles) and the lowest root mean square error of prediction (RMSEP) value was chosen. For WAPLS, to avoid overfitting the data, improvements in RMSEP of less than 5% between successive model components were deemed insignificant (ter Braak & Juggins, 1993). This decision path was only applied to the first three components to limit complexity of the statistical analysis (Wright et al., 2011; Barlow et al., 2013).

We applied the foraminifera-based transfer function to fossil foraminiferal assemblages from three cores from Mission Bay (see the following section). We use the modern analogue technique (MAT) to quantify the resemblance between each fossil sample and the modern training set (Birks, 1998;

Kemp & Telford, 2015). We selected the squared chord distance (Overpeck et al., 1985) for the calculation of minimum dissimilarity coefficient (MinDC). The 20th percentile of dissimilarity values between all possible pairings of modern samples was selected as the threshold (Watcham et al., 2013). Samples with dissimilarity coefficients lower than the 20th percentile were defined as having close analogues and samples with coefficients greater than the 20th percentile as having no close analogues.

#### STRATIGRAPHY, CHRONOLOGY AND FOSSIL FORAMINIFERA

To provide an initial test of the applicability of the modern training set for reconstructing depositional elevations from fossil salt-marsh sequences, we investigated the stratigraphy of the Mission Bay salt marsh. The subsurface sediment was described from 10 hand-driven cores collected in the northern and western parts of the marsh (Fig. 1; Appendix 2). These cores were collected in overlapping, 50-cm-long sections using a Russian corer to avoid compaction. Selected core sections were wrapped, labelled, and kept alongside all surface samples in a refrigerator at 4°C prior to laboratory analyses. The stratigraphy was documented along two transects: an east to west transect and a north to south transect (Fig. 1D). The latter transect is oriented in the same direction as cores described by Scott et al. (2011). The stratigraphy is based on the characterization of the sedimentary facies described in all cores, and the lateral stratigraphic relations between them. Each sedimentary facies was described based on its observable physical features, such as sediment type, color, texture (grain-size, sorting), and fossils.

Three cores from the eastern part of the marsh were selected for analysis. Their selection was based on a reconnaissance survey, analysis of aerial photography, and a historical map from 1852 that indicated minimal human modification during the 20th century and that the sites were far from river channels and/or tidal flats (Figs. 1D–E). Core MB17-05 was selected for foraminiferal analysis and dating on the basis of its position in the high marsh zone, and thus it includes the thickest and most continuous sequence of salt-marsh sediment accumulation overlying incompressible basement rock. Cores MB17-08 and MB17-07 were chosen for comparison with MB17-05, aiming to replicate the results from core MB17-05. Sampling for fossil foraminifera followed the approach applied to the surface samples.

We developed a chronology for cores MB17-05 and MB17-08 based on  $^{14}\text{C}$  dating,  $^{210}\text{Pb}$  analysis and  $^{137}\text{Cs}$  age markers. For  $^{14}\text{C}$  dating, we sampled identifiable above-ground material from terrestrial plants to avoid erroneously

young dates from root matter. Samples were washed in deionized water, dried at 70°C for 24 hours, and transported to the University of California, Irvine Keck Radiocarbon Laboratory, where they were cleaned, combusted, and graphitized before undergoing accelerator mass spectroscopy (AMS). Values of  $^{137}\text{Cs}$  and  $^{210}\text{Pb}$  were measured using an Ortec germanium crystal well detector at the PEARL Laboratory at Queen's University, Kingston, Ontario using methods from Schelske et al. (1994). A total of 18 samples were tested for gamma activity in core MB17-05, the thickest marsh record, and seven samples were tested along the core length of MB17-08 to determine the basic profile shape, to be compared with MB17-05. We developed Bayesian age-depth models using the *rplum* package (Blaauw et al., 2022) within the R environment (R Core Team, 2013), incorporating the  $^{137}\text{Cs}$ ,  $^{210}\text{Pb}$ , and  $^{14}\text{C}$  results. This approach alleviates the need to remodel outputs from traditional  $^{210}\text{Pb}$  depositional models (Aquino-López et al., 2018, 2020). Radiocarbon dates were calibrated within *rplum* using the IntCal20 calibration curve (Reimer et al., 2020). We included boundaries at key stratigraphic transitions to allow greater model flexibility and adjusted depths to account for any abruptly deposited units.

## RESULTS

### CONTEMPORARY FORAMINIFERAL ASSEMBLAGES

Figure 2 summarizes the distribution of the dominant taxa identified from the Mission Bay and Carpinteria Slough salt marshes. Twelve different agglutinated taxa occur in the dead populations from the two sites (Figs. 2, 3, Appendices 3 and 4). Among the most abundant species, *Entzia macrescens* and *Trochammina inflata* occur at both sites, while *Balticammina pseudomacrescens* and *Haplophragmoides wilberti* occur only in samples from Carpinteria Slough. *Balticammina pseudomacrescens* occurs at six stations; its highest concentrations occur at two stations in the high marsh where its relative abundance ranges between 40 and 50% of the total assemblage composition. *Miliammina fusca* also occurs at both sites; however, the highest concentrations occur in samples from Carpinteria Slough. The most common species exhibit observable zonation relative to elevation, which follows the vascular plant zonation in both the studied marshes (Appendix 5).

We combine the samples from Mission Bay and Carpinteria Slough with published assemblage data from Seal Beach and Tijuana to form an 89-sample regional modern training set (Fig. 4). Elevation dependent zonation in this dataset is revealed by the Q-mode cluster analysis. Three main clusters are identified at a Bray-Curtis similarity of 60%, with one of the clusters further divided into two subclusters (Fig. 4). Cluster 1 mostly contains samples from the unvegetated tidal flat at Carpinteria Slough, with two samples from the low marsh or tidal flat/marsh transition (Appendix 5). Elevations range between 88 and 174 SWLI units. At these lowest elevations *M. fusca* (25–99%, 71% on average) and calcareous species (max of 68%, 25% on average) dominate the assemblages (Fig. 4). Cluster 2 represents two samples from middle to high marsh in Carpinteria Slough. These samples were differentiated from cluster 3 by their excep-

tional abundance of *Balticammina pseudomacrescens*, reaching 52%. Subcluster 3a consists of low to middle marsh samples from all four sites, with elevations between 123 and 211 SWLI units. The most important foraminiferal species contributing to this sub cluster are *E. macrescens* (6–90%, 45%±26% on average) and *T. inflata* (5–63%, 32%±17% on average). *Miliammina fusca*, *H. wilberti* and calcareous species also occur but in lower abundances (<10% on average). These elevations are often dominated by the low marsh plant *Spartina* spp., which is accompanied middle marsh plants such as *Sarcocornia pacifica*, *Batis maritima*, and *Jaumea carnosa* in some areas (Appendix 5). Subcluster 3b comprises samples from the middle to high marsh elevations from three marsh sites, excluding Carpinteria Slough. Sample elevations in this cluster are above 167 SWLI units. These samples have similar contributions of *E. macrescens* and *T. inflata* as in subcluster 2a; however, they also include less common species, such as *Trochammina irregularis* and *Miliammina petila* (both <15%). These elevations are typically characterized by the high marsh plants *Distichlis spicata*, *Frankenia grandifolia*, *Limonium californicum*, and *Arthrocnemum subterminale*, occasionally alongside mid-marsh plants (Appendix 5).

The length of the first DCCA axis 1, 2.457 standard deviation units, indicates a unimodal rather than a linear relationship between foraminifera and elevation in the regional modern training set. Consequently, we use a unimodal ordination method, CCA. The CCA results suggest a significant influence of elevation on the species distributions in the modern data set (Fig. 5). Elevation explains 16% of the cumulative variance of the foraminiferal data (Fig. 5). *Miliammina petila* and *T. irregularis* occur at high marsh stations and are positively correlated with elevation. Conversely, *M. fusca*, *Scherochorella moniliformis*, and calcareous species are present in the low marsh to tidal flat stations and are negatively correlated with elevation. *Entzia macrescens* and *T. inflata* occur in variable relative abundances at all marsh sites and do not seem to be closely correlated with elevation.

### MISSION BAY STRATIGRAPHY AND BIOSTRATIGRAPHY

The sedimentary sequence in the main east to west transect (Figs. 1D, 6) consists of a basal incompressible bedrock (documented in cores MB17-04, MB17-05, and MB17-06) overlain by gray silty sand, barren of any faunal remains. The barren gray silty-sand was found in all of the E-W transect cores apart from MB17-04 (Fig. 6). Both of these sedimentary facies (#8 and #9 in Fig. 6) represent middle to late Pleistocene-aged paralic deposits. Grayish sandy-clayey silt with some organics and scarce agglutinated salt-marsh foraminifera (facies #7) overlie the basal sediments in most of the cores (excluding MB17-04 and MB17-06). The overlying sequence consists of gray-brown organic sandy-clayey silt (facies #2) interrupted in most of the cores by two light gray organic sandy-clayey silt beds (facies # 4) with sharp upper and lower contacts. Core MB17-05 contains only the upper silt layer, but also features a younger unit of grey-brown silty-clayey sand (facies #3). The uppermost part of the sequence (between 10 and 37 cm in thickness) is com-

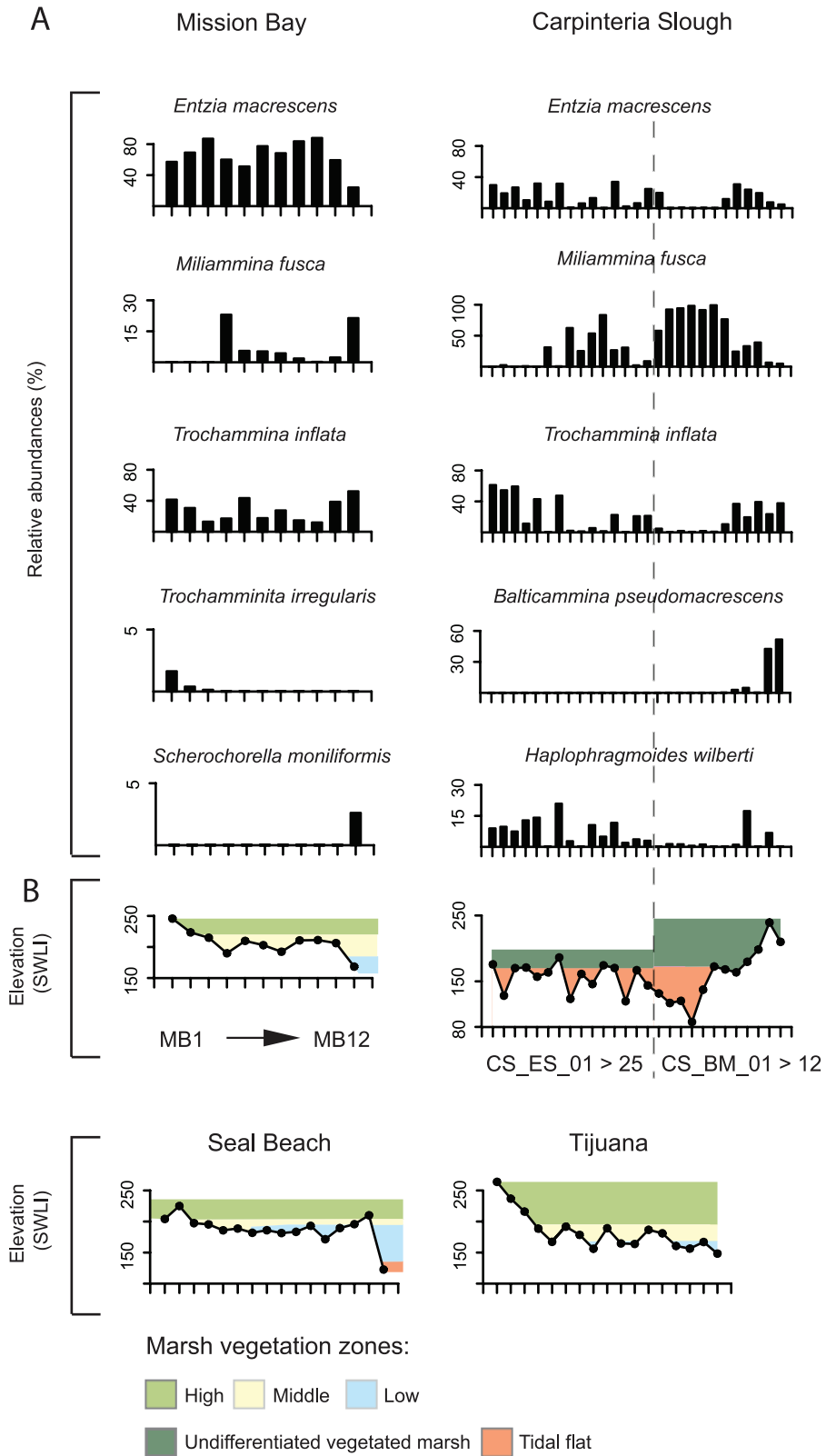


FIGURE 2. A) Relative abundances of dead foraminifera in the Mission Bay and Carpinteria marshes. B) Sample elevation profiles with illustration of plant zonation at Mission Bay, Carpinteria, Seal Beach, and Tijuana. Note, in all transects, samples were not taken at even distances. Dashed line separates different transects at Carpinteria Slough.

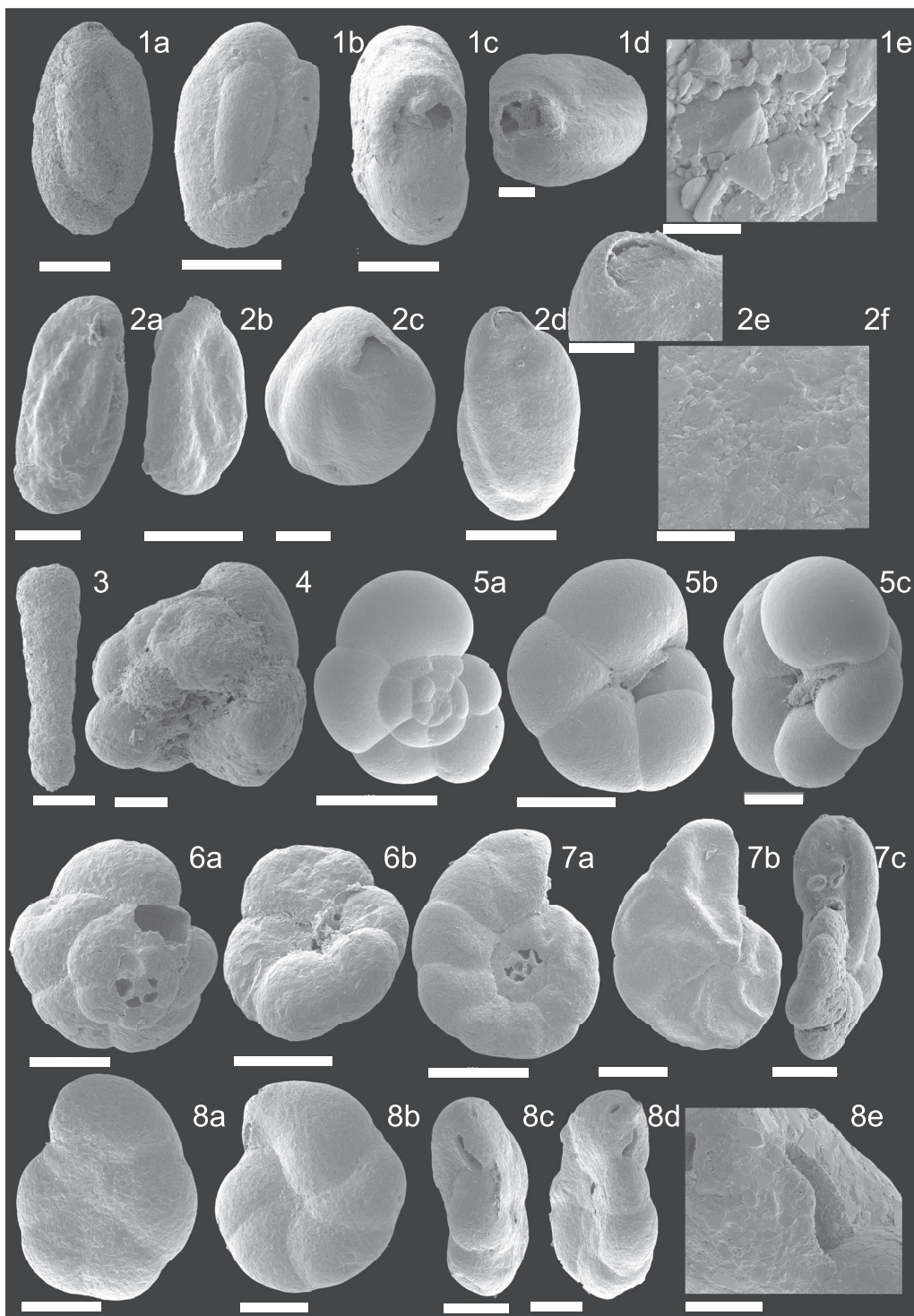


FIGURE 3. Scanning electron micrographs of agglutinated foraminifera from surface and subsurface sediments collected in the study areas along the coast of southern California. The scale bars of Figs. 1e, 2f equal 5  $\mu\text{m}$ , of Fig. 2e equals 30  $\mu\text{m}$ , of Fig. 8e equals 40  $\mu\text{m}$ , of Figs. 1d, 2a, 2c equal 50  $\mu\text{m}$ , of Figs. 1c, 2b, 2d, 3, 4, 6a-b, 7b-c, 8a-d equal 100  $\mu\text{m}$ , of Figs. 1a-b, 5b-c, 7a equal 200  $\mu\text{m}$ , of Fig. 5a equals 400  $\mu\text{m}$ . **1a-b** *Miliammina fusca* (Brady, 1870), side view. **1c-d** *M. fusca*, aperture view slightly clogged, yet showing no tooth. **1e** *M. fusca*, focus on siliceous wall composed of small quartz grains with almost no cement giving the species rough surface appearance. **2a-b** *Miliammina petila* Saunders, 1958, side view showing a more elongate and smaller test compared to the latter species. **2c** *M. petila*, aperture view showing approximately equal width and thickness of the test. **2d-e** *M. petila*, aperture views showing much broader tooth than the latter species, which almost fills the aperture. **2f** *M. petila*, focus on siliceous wall composed of minute quartz grains in a large amount of siliceous cement giving the species smoother surface appearance. **3** *Scherchorella moniliformis* (Siddall, 1886), side view. **4** *Trochammina irregularis* Cushman & Brönnimann, 1948, side view. **5a** *Trochammina inflata* (Montagu, 1808), spiral view. **5b** *T. inflata*, umbilical view. **5c** *T. inflata*, aperture view. **6a** *Siphotrochammina lobata* Saunders, 1957, spiral view. **6b** *S. lobata*, umbilical view. **7a** *Entzia macrescens* (Brady, 1870), spiral view. **7b** *E. macrescens*, umbilical view. **7c** *E. macrescens*, aperture view with secondary apertures. **8a** *Arenoparrella mexicana* (Kornfeld, 1931), spiral view. **8b** *A. mexicana*, umbilical view. **8c-e** *A. mexicana*, aperture view.

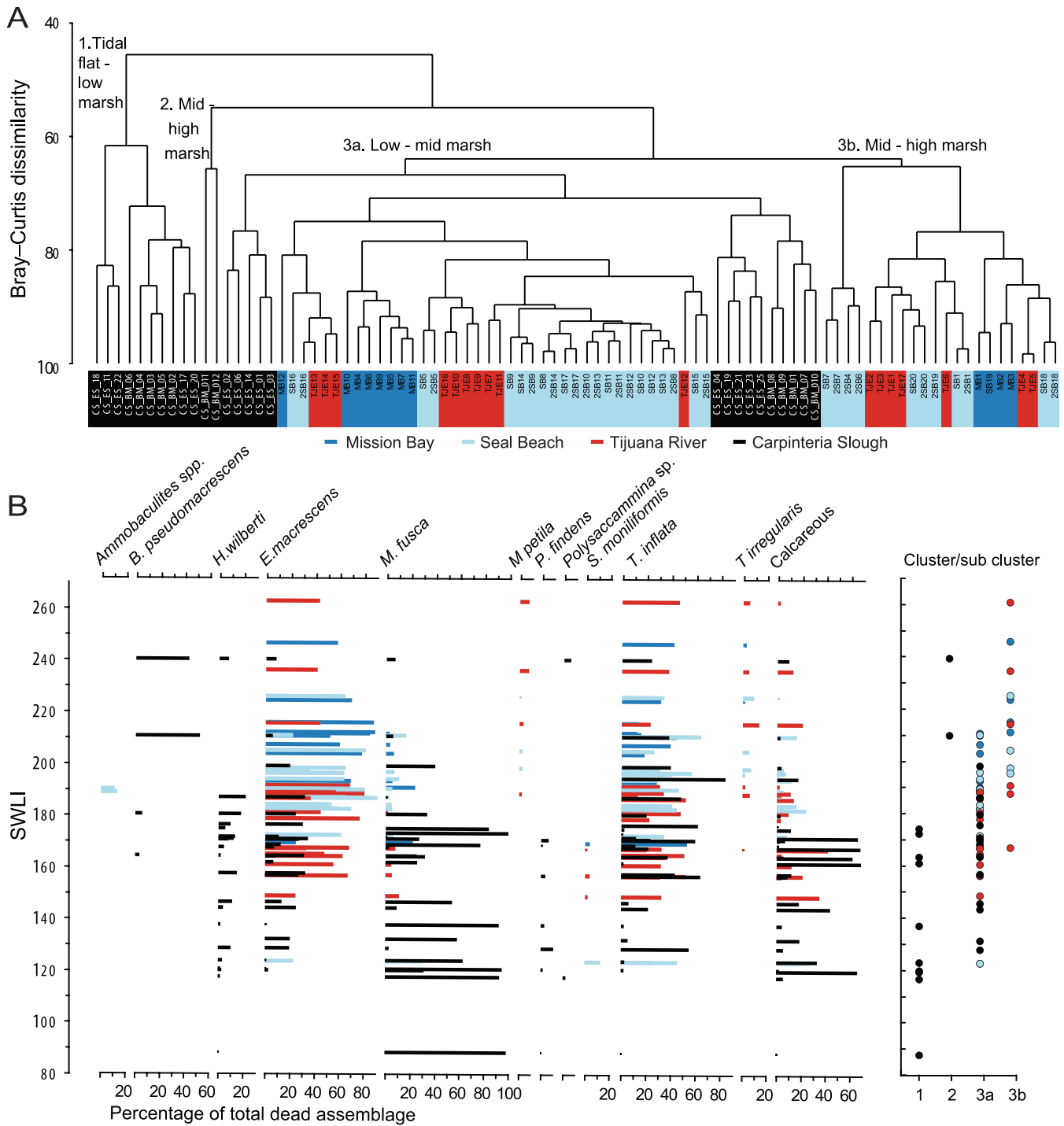


FIGURE 4. A) Dendrogram of Q-mode cluster analysis of the dead foraminifera from the four marshes: Mission Bay, Carpinteria Slough, Seal Beach, and Tijuana. B) Modern foraminiferal data for the four marshes, showing taxa exceeding 5% of total tests in at least one sample. Samples are ordered by elevation using the standardized water level index (SWLI), and species are ordered by elevation optima as calculated by weighted averaging.

posed of brown highly organic rooted (peat-like) salt-marsh sediment (facies #1).

Cores MB17-05, MB17-07, and MB17-08 were selected as representative of the stratigraphy and subjected to microfossil analyses. Core MB17-05 contains the thickest section of salt-marsh sediment with a continuous high concentra-

tion of agglutinated foraminifera down to 140 cm (Fig. 7A). Below this depth, in the basal silt and sandy-clayey silt, foraminifera are absent. *Trochammina inflata* and *E. macrescens* dominate the overlying organic salt-marsh deposits, accompanied by *M. petita* and *Arenoparrella mexicana* (Fig. 7A). The latter species occurs in all sampled cores

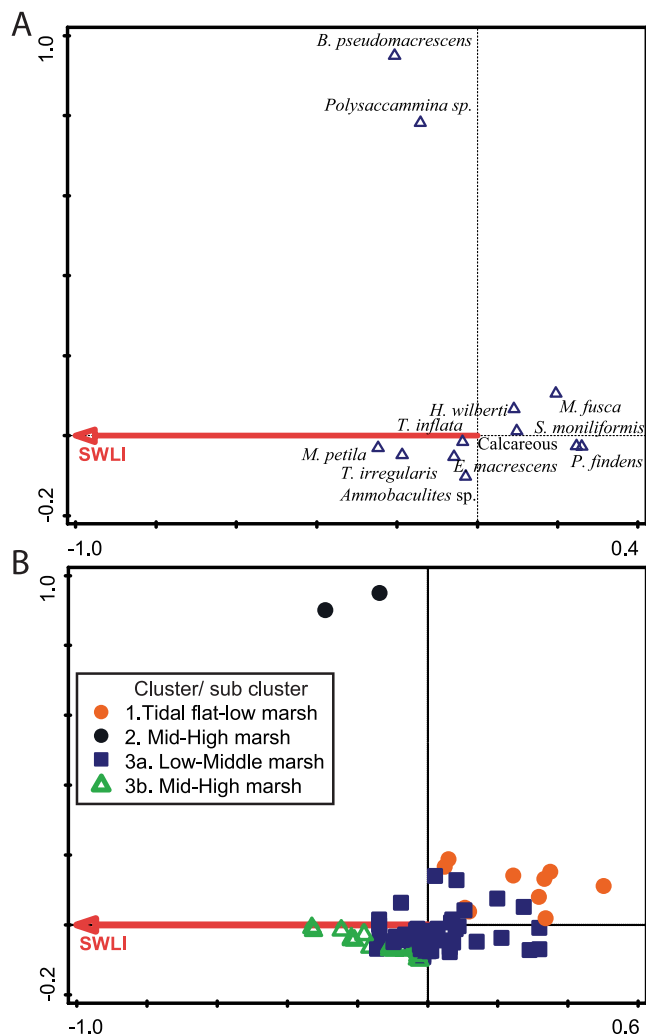


FIGURE 5. Canonical correspondence analysis (CCA) ordination biplots with forward selection of elevation as the significant environmental variable ( $p < 0.05$ ) showing retrospective projection of the surface species—elevation (A) and samples—elevation (B) for the combined data sets of Mission Bay, Carpinteria Slough, Seal Beach, and Tijuana.

only below 40 cm. Between 50 and 40 cm core depth, *M. fusca* increases at the expense of *E. macrescens*. The species is dominant in the light grey organic sandy-clayey silt layer (facies #4) before declining in the overlying sediments and being replaced by *E. macrescens* and *T. inflata*. The transition to sedimentary facies #3 in core MB17-05 is characterized by the complete disappearance of foraminifera, before a return to an assemblage dominated by *E. macrescens* and *T. inflata* in sedimentary facies #1 (Fig. 7A).

Foraminiferal assemblages in cores MB17-07 and MB17-08 are also dominated by *T. inflata* and *E. macrescens*, with *A. mexicana* encountered below 50 cm core depth (Figs. 7B, C). As in the equivalent layer of facies #4 in core MB17-05, *M. fusca* increases in the upper light grey organic sandy-clayey silt in cores MB17-07 and MB17-08. The lower layer of this facies in core MB17-08, which is absent in MB17-05, displays an abrupt increase in *M. fusca* coincident with the stratigraphic boundary. Although sampled at lower res-

olution, this abrupt change is replicated in core MB17-07, where *M. fusca* is absent in the underlying sediments but exceeds 50% of the assemblage in the light grey silt unit.

#### CORE CHRONOLOGY

Radiocarbon results are presented in Table 2 and plotted alongside the stratigraphy in Figure 6. Radionuclide results and age-depth models are presented in Figure 8. The lack of suitable plant macrofossil samples at key depths limits the ability of the age-depth model to constrain the timing of the stratigraphic boundaries. While we provide initial age estimates in the following sections, further dating is required to enhance the chronological framework.

Activity of  $^{137}\text{Cs}$  is low through most of core MB17-05 with a small peak between 28–36 cm depth. The *rplum* model indicates that this peak is an outlier and significantly younger than the ages inferred from the  $^{210}\text{Pb}$  and  $^{14}\text{C}$  results (Fig. 8A). Low  $^{137}\text{Cs}$  fallout means that records from Southern California can be unreliable (Drexler et al., 2018); however, the occurrence of  $^{137}\text{Cs}$  at deeper than expected depths may also point towards post-depositional mobility in the sediment profile (Foster et al., 2006). Core MB17-08 presents a clearer peak in  $^{137}\text{Cs}$  activity at 15 cm depth (Fig. 8B), and the age-depth model indicates that this is consistent with the other chronological data from this core.

#### DISCUSSION

##### MODERN FORAMINIFERAL DISTRIBUTIONS

The tidal flat and low marshes of the study sites are characterized by the presence of the agglutinants *M. fusca* and *S. moniliformis* and several calcareous species. These agglutinants are known as lower-elevation species along, for example, the North American Pacific and Atlantic coasts (e.g., Edwards et al., 2004; Nelson et al., 2008; Milker et al., 2015; Avnaim-Katav et al., 2017). In the middle marsh and the high marsh, the dominant species include *T. inflata* and *E. macrescens*. Their distribution is similar to other studies. For example, in Australia and other areas in North America, *E. macrescens* and *T. inflata* have been reported from middle marsh environments (Guilbault et al., 1996; Nelson et al., 2008; Hawkes et al., 2010; Engelhart et al., 2013; Milker et al., 2015) and the highest marsh positions (e.g., Patterson, 1990; Gehrels & van de Plassche, 1999; Hippensteel et al., 2002; Woodroffe & Horton, 2005). Some of the highest elevation samples in this study included *T. irregularis* and *M. petila*. These species have frequently been identified as the dominant species in the high and highest positions within North American Pacific salt marshes (Hawkes et al., 2010; Engelhart et al., 2013; Milker et al., 2015), as well as in New Zealand (Southall et al., 2006) and Tasmania (Callard et al., 2011). Likewise, *M. petila* has also been reported in the middle and high marshes from Oregon (Engelhart et al., 2013).

The zonation in modern foraminiferal assemblages from the four salt marshes confirms their potential for being used as accurate and precise indicators of depositional elevations. Clusters of samples defined by Q-mode cluster analysis overlap but can be related to different marsh elevation zones (Fig. 4). While elevation explains 16% of the variance in the re-

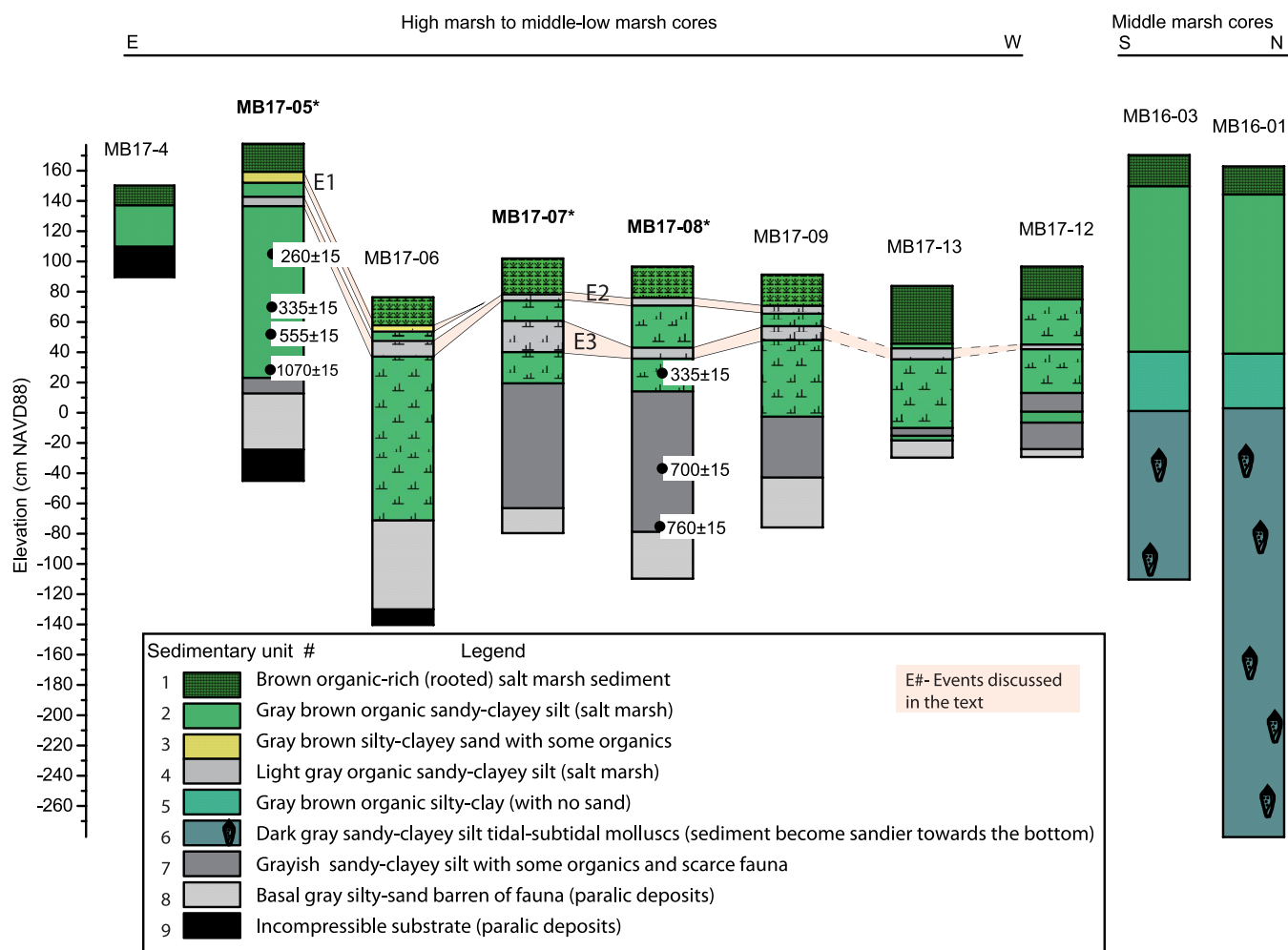


FIGURE 6. Mission Bay salt-marsh stratigraphy described from selected cores recovered along an east to west transect and a north to south transect. Cores named in bold and marked with an asterisk were selected for detailed analysis. Sedimentary facies are numbered in the legend.

gional training set, this result is similar to other studies from Canada, Oregon, USA and the UK (e.g., Barnett et al., 2016; Hawkes et al., 2010; Horton & Edwards, 2006), and not unexpected given that other variables, such as salinity and grain size, also influence foraminiferal distributions (Horton et al., 1999; Horton & Edwards, 2006; Avnaim-Katav et al., 2017).

#### TRANSFER FUNCTION DEVELOPMENT

As DCCA results indicate a unimodal species response in the regional training set, we develop transfer functions using unimodal regression models (i.e., WA, WAPLS, and LWVA). We do not develop a local transfer function model for Mission Bay due to the low number of modern samples from the site. The LWVA transfer function with inverse deshrinking provides the best performance, with a strong relationship between observed and predicted elevations (Fig. 9). The residual scatter suggests that some elevation predictions are underestimated, particularly from the landward upper edge of the gradient (high marsh).

The RMSEP, 22 SWLI units, is equivalent to 0.18 m at Mission Bay and is 16% of the sampled elevation range.

These values accord well with the ranges discussed by Callard et al. (2011), Barlow et al. (2013), and Williams et al. (2021).

#### COMPARISON OF MODERN AND FOSSIL ASSEMBLAGES

Reliable reconstructions of paleo-marsh elevation and consequently relative sea-level or land-level change depend on the presence of similar assemblages in the contemporary and fossil data sets and that the species' responses to the environment haven't changed during the course of time. Our MAT results show that the modern training set provides 69 out of the 101 fossil samples in the three cores from Mission Bay with close analogues (Figs. 7). The largest number of poor analogues occur in the lower parts of the high marsh core, MB17-05, at the eastern end of the transect (23 poor analogues out of 56 samples; Fig. 7A). This is largely due to the presence of *Arenoparrella mexicana*, which is absent in the modern data set. This species is known from mangrove environments living in the subtidal zone, for example in southern Brazil (Barbosa et al., 2005) or in the upper intertidal zone in Australia (Berkeley et al., 2008). It is also found

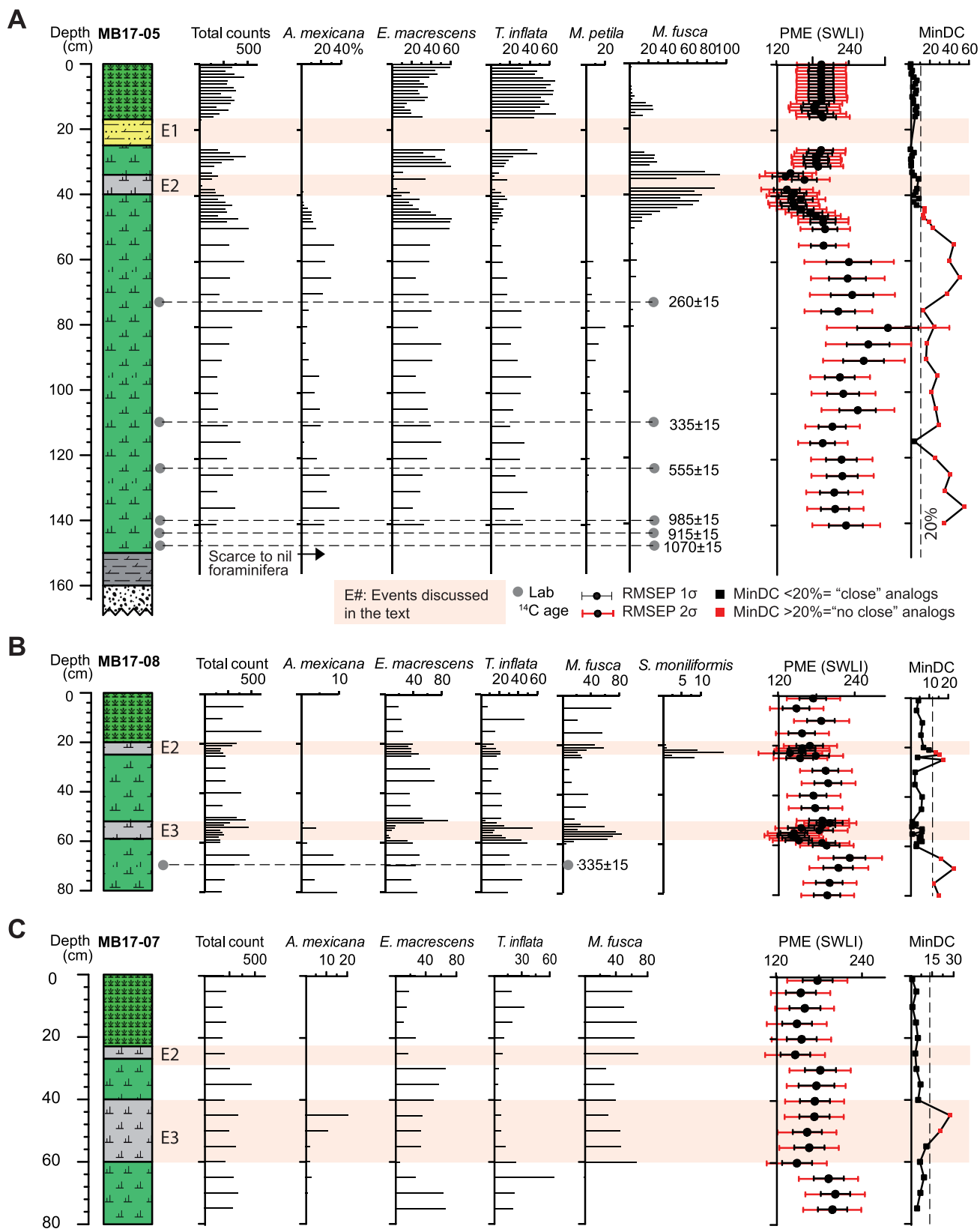
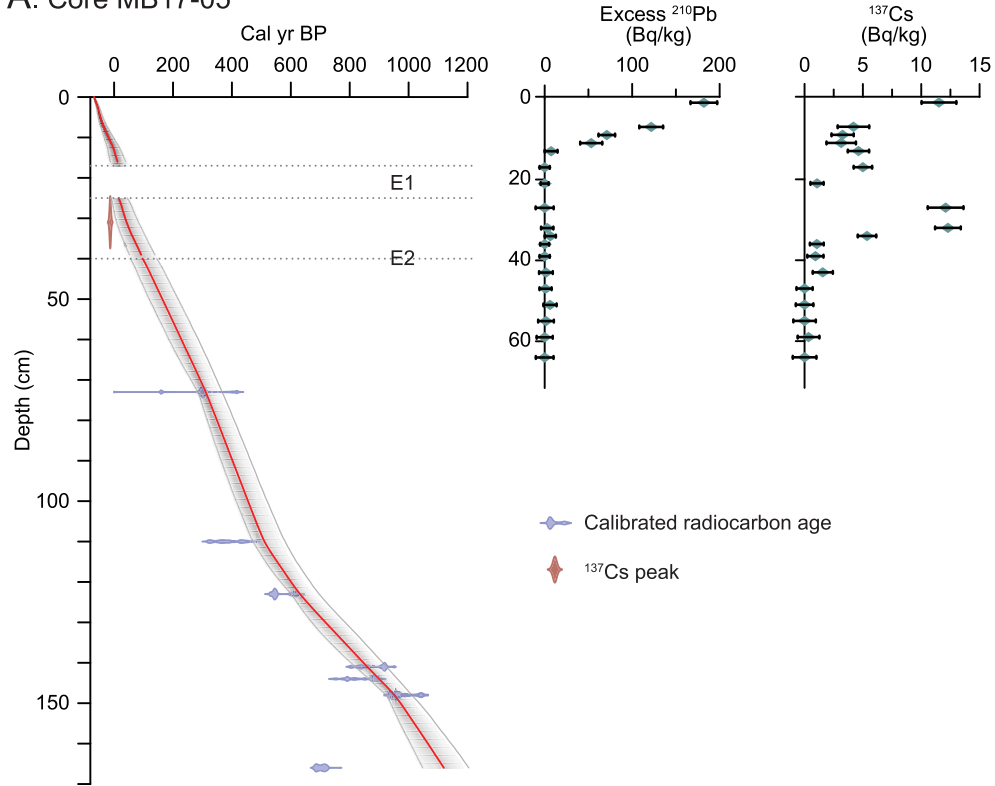


FIGURE 7. Relative abundances of dead foraminifera from cores MB17-5 (A), MB17-08 (B) and MB17-07 (C), including counts, percentages of the common species and paleo-marsh elevations (SWLI units) with sample specific errors of prediction (1 sigma – black bar, 2 sigma – red bar) calculated with the foraminifera-based Locally Weighted Weighted Averaging transfer function. Results of the Modern Analog Technique are also shown. For the sedimentological legend see Figure 6. For cores MB17-08 and MB17-07, only the foraminifera-bearing units are displayed; the barren underlying units are shown in Figure 6.

A. Core MB17-05



B. Core MB17-08

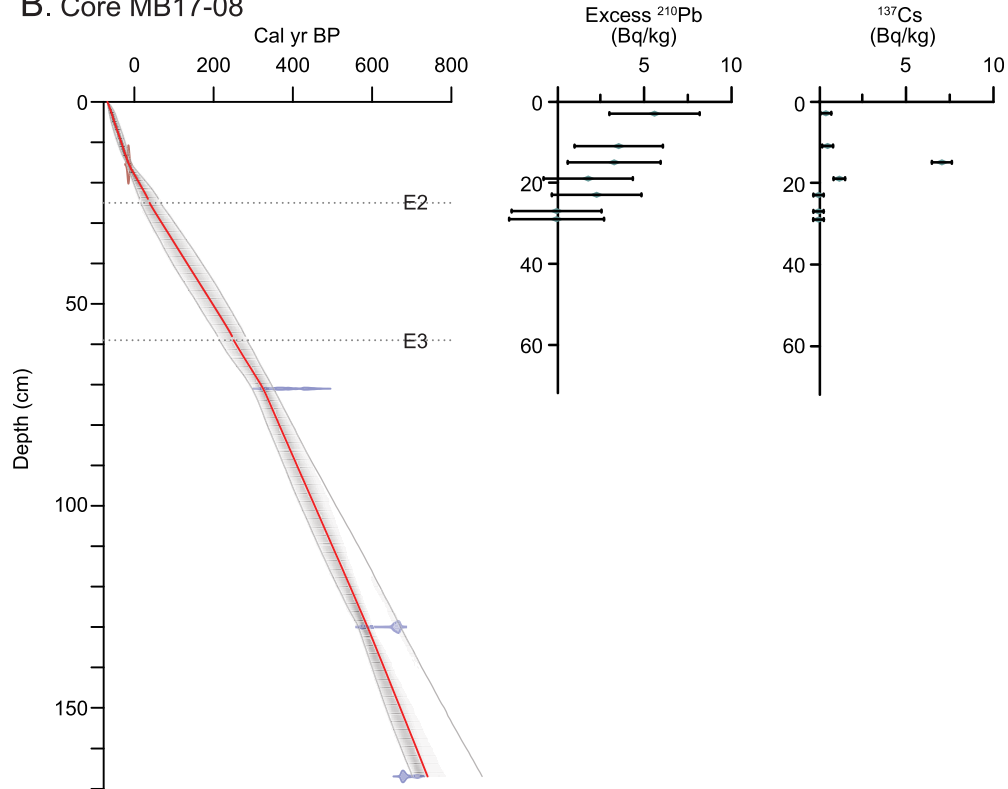


FIGURE 8. Bayesian age-depth models for cores MB17-05 (A) and MB17-08 (B) produced in the R package rplm (Blaauw et al., 2022). Excess  $^{210}\text{Pb}$  and  $^{137}\text{Cs}$  activities ( $\text{Bq kg}^{-1}$ ) are presented to the right-hand side of the models. The 95% confidence interval for the age-depth model is outlined in grey and the most likely age-depth model is plotted in red. Individual MCMC iterations of possible age-depth modes are drawn on the plot and darker grey areas indicate more likely calendar ages.

TABLE 2. AMS  $^{14}\text{C}$  dating results. All samples consisted of plant macrofossils. Ages are calibrated using the IntCal20 calibration curve (Reimer et al., 2020). Calibrated ages show time intervals of >95% probability distribution at 2 sigma ranges.

Lab ID (UCIAMS #)	Core depth (cm)	$^{14}\text{C}$ age (yr BP)	Calibrated age (yr CE, $2\sigma$ )
<i>Core MB17-05</i>			
185592	73	260 ± 15	1530–1537 (4%) 1636–1663 (90%)
191928	110	335 ± 15	1786–1794 (6%) 1490–1529 (29%) 1538–1604 (50%)
185593	123	555 ± 15	1606–1635 (21%) 1326–1352 (30%) 1394–1421 (70%)
185594	141	985 ± 15	1022–1048 (54%) 1082–1129 (39%) 1138–1151 (7%)
191929	144	915 ± 15	1043–1087 (55%) 1092–1106 (5%) 1117–1178 (37%) 1192–1202 (3%)
191930	148	1070 ± 15	899–919 (16%) 958–967 (3%) 974–998 (45%) 999–1022 (35%)
185595	158	790 ± 15	1224–1271 (100%)
<i>Core MB17-08</i>			
191931	71	335 ± 15	1490–1529 (29%) 1538–1604 (50%) 1606–1635 (21%)
191932	130	700 ± 15	1277–1300 (95%) 1372–1376 (5%)
191933	167	760 ± 15	1229–1245 (11%) 1256–1281 (89%)

in the Great Marshes of Massachusetts; however, there it does not demonstrate vertical zonation (de Rijk & Troelstra, 1997). In a Georgia salt marsh, it is more abundant as an infaunal species in the high-marsh subsurface than in surface samples where it is generally absent (Goldstein & Harben, 1993). In the Morbihan Gulf marshes along the Atlantic coast of SW Europe, this species was recorded mostly in stations slightly below MHHW (Leorri et al., 2010). The absence of consensus in the literature about the distribution of this species and the potential for infaunality mean samples containing this species should be treated cautiously when estimating paleo-marsh elevations. Future research should seek to resolve the distribution of *A. mexicana* in southern California.

#### CORE CHRONOLOGY

We use *rplum* to create age-depth models which integrate results from  $^{137}\text{Cs}$ ,  $^{210}\text{Pb}$ , and  $^{14}\text{C}$  methods. As suitable radiocarbon samples closely bracketing E1, E2, and E3 were not encountered and the depositional environment of California coastal marshes can present challenges when using  $^{137}\text{Cs}$  or  $^{210}\text{Pb}$  (Drexler et al., 2018), the ages presented here for the events remain somewhat uncertain. In particular, the timing of E2 in core MB17-05 (estimated by the age-depth model as 1805–1894 CE) is poorly constrained as it lies below the limit of significant  $^{210}\text{Pb}$  activity and more than 30 cm above the nearest radiocarbon date. If this sedimentary transition is indeed synchronous between cores, the age derived from core MB17-08 (1885–1934 CE) would be

preferred as it is better constrained by the available chronohorizons. A more conservative interpretation would place this transition before ~1900 CE—the time at which excess  $^{210}\text{Pb}$  can be detected (Jeter, 2000)—but after 1530–1794 CE.

While our models do make allowances for abruptly deposited units, particularly E1 as discussed in the following section, the lack of ages closely bracketing the events prevents us from making inferences about the duration of any hiatuses in sediment deposition or the occurrence of erosion. Future sampling could focus on obtaining dates from immediately above and below each boundary; this would allow alternative approaches such as Sequence modelling to refine the age estimates (cf. Lienkaemper & Bronk-Ramsey, 2009; Shennan et al., 2014).

#### RECONSTRUCTING LATE HOLOCENE PALEOENVIRONMENTAL CHANGES IN MISSION BAY

We use the transfer function outlined above (section ‘Transfer function development’) to calibrate the fossil assemblages in the three cores (Fig. 7). Throughout the salt-marsh sequence, reconstructed paleo-marsh surface elevations range from approximately 130 to 270 SWLI units, equivalent to ~1–2 m above MTL, assuming that the tidal range has not changed over time. While these marsh surface elevations could be combined with the age-depth model described in section ‘Core chronology’ to realize a relative sea-level reconstruction, such a step is complicated at present by our incomplete knowledge of geomorphic changes at the site. Such changes, including those linked to rerouting of the

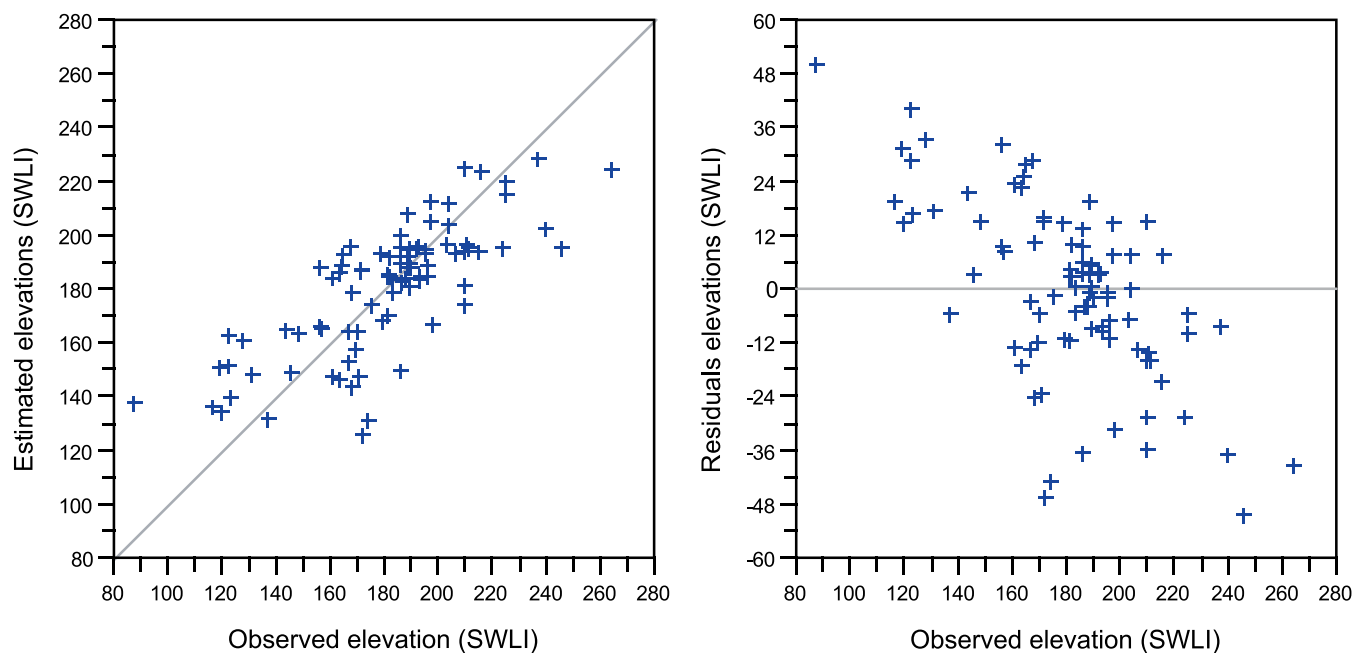


FIGURE 9. Scatterplots showing the relationship between observed elevations (SWLI, standardized water level index) and model predicted elevation (left panel) and observed elevation versus residuals (right panel) using the Locally Weighted Weighted Averaging transfer function.

San Diego River, sediment infilling, and dredging may have resulted in substantial changes to the tidal range over time and therefore altered the conversion of SWLI values into meters. Consequently, rather than focusing on the long-term changes in relative sea level, we concentrate on the origin of the intercalated layers within sedimentary facies #2.

Three notable changes in stratigraphy occur within the salt-marsh sediments of sedimentary facies #2. The oldest transition is recorded in mid and low marsh cores, including MB17-07 and MB17-08, as a change in the color of the organic sandy-clayey silt, accompanied by an abrupt increase in the relative abundance of the low marsh species *M. fusca* and a decline in the mid to high marsh *E. macrescens* and *T. inflata* (Figs. 7B, C). Assuming no simultaneous change in tidal range, reconstructed palaeomorph surface elevations indicate an abrupt decrease in paleomorph surface elevation of  $0.71 \pm 0.26$  m in core MB17-08 and  $0.41 \pm 0.24$  m in core MB17-07. It should be noted that the reconstruction for core MB17-08 is reliant on a sample that lacks a close modern analogue due to the contribution of *A. mexicana* (discussed in section ‘Comparison of modern and fossil assemblages’). The age model for MB17-08 indicates this transition, which we refer to as event 3 or E3, occurred at 215–284 cal yr BP (1666–1735 CE; Fig. 8).

A second change in marsh stratigraphy is recorded in all three sampled cores, again primarily as a change in the color of the organic sandy-clayey silt. While cores MB17-05 and MB17-08 both see an increase in *M. fusca* across the contact, the increase in this low marsh species is gradual, starting 10 cm below the change in sediment color in MB17-05. A corresponding increase in *M. fusca* in core MB17-07 is also evident, but the abrupt or gradual nature of the change is less clear due to the lower sampling resolution. Reconstructed paleomorph surface elevations show a gradual decrease ranging between  $\sim 0.2$  and 0.5 m in the three cores analyzed. The

age models suggest that the stratigraphic transition, E2, occurred at 56–145 cal yr BP (1805–1894 CE) in MB17-05 and 16–65 cal yr BP (1885–1934 CE) in MB17-08 (Fig. 8).

A third environmental change, E1, is recognized as an organic–minerogenic contact occurring only at the eastern edge of the marsh in core MB17-05 (Fig. 7A). The silty-clayey sand deposits of sedimentary facies # 3 lack lateral continuity between cores and are devoid of foraminifera. Under and overlying sediments contain similar assemblages dominated by the mid to high marsh foraminifera *E. macrescens* and *T. inflata*, with no difference in reconstructed paleomorph surface elevation. The age model indicates the sand was deposited between -10 and 45 cal yr BP (1905–1960 CE; Fig. 8).

#### POTENTIAL ORIGIN OF ENVIRONMENTAL CHANGES E1 – E3

Coseismic deformation on the Newport–Inglewood–Rose Canyon fault zone is unlikely to produce any significant vertical deformation in the study area due to the strike-slip fault motion (Lindvall & Rockwell, 1995; Rockwell, 2010). Nevertheless, earthquake shaking-induced lateral spreading could result in abrupt changes in paleomorph surface elevation. Such an occurrence would be expected to share characteristics more usually associated with upper plate deformation in subduction zone settings, including lateral continuity of stratigraphic evidence between cores, evidence for a sudden change in marsh elevation and synchronicity with other evidence for earthquake occurrence (Nelson et al., 1996; Shennan et al., 2016). As E3 can be traced across multiple cores and displays foraminiferal evidence for an abrupt, decimeter-scale decrease in marsh elevation, we hypothesize that the stratigraphy might record the secondary effects of earthquake shaking. Paleoseismic trenching across the Rose Canyon fault in the Old Town

area of San Diego documented four large and two smaller late Holocene surface-rupturing events, with the most recent earthquake occurring between 1704 CE and the mid-1700s (Grant & Rockwell, 2002; Singleton et al., 2019). The timing of this earthquake correlates well with our preliminary age assessment for E3 (1666–1735 CE). We suggest shaking-induced lateral spreading could have resulted in an abrupt decimeter-scale decrease in marsh surface elevation, and a sudden consequent change in foraminiferal assemblages in the Mission Bay marsh. A similar analogue for such a mechanism occurred during the 1999 İzmit earthquake, Eastern Turkey, where liquefaction-induced lateral spreading resulted in submergence of coastal areas (Aydan et al., 2008). While the event predates the start of substantial anthropogenic impacts in Mission Bay, further work is needed to rule out the possibility of other causal processes, such as non-seismic geomorphic changes or anthropogenic impacts. Additional mapping of the stratigraphic change and further quantification of the amount and abruptness of the possible elevation change from additional cores would also help to support or refute the hypothesized process.

The foraminiferal changes associated with E2 and E1 are not consistent with the mechanism proposed for E3. Event 2, tentatively dated to the 19<sup>th</sup> to early 20<sup>th</sup> century, lacks evidence for an abrupt change in marsh elevation. Instead, the gradual change observed in assemblage composition, including the increased abundance of *M. fusca* that dominates lower elevations may reflect anthropogenic changes to the geomorphology and tidal range in Mission Bay, in particular following the rerouting of the San Diego River's course into the bay in 1850 (Marcus, 1989). As E1 lacks widespread lateral continuity and evidence for marsh surface elevation change, fluvial flooding provides one plausible formation mechanism. The age range (1905–1960 CE) coincides with the 1938 CE floods, which resulted from a series of tropical storms (the Lash of Saint Francis) that were the largest floods in the history of southern California and covered coastal areas of Los Angeles, Orange, and Riverside Counties with >1-m thick deposits of silty sand (Poland & Piper, 1956). Further mapping and sedimentological analyses could help to confirm the origin of this layer.

## CONCLUSIONS

To investigate the control of elevation, a surrogate for the frequency and duration of tidal inundation, on the distribution of salt-marsh foraminifera in Southern California, we quantified faunal assemblages in surface samples along transects from marshes at Mission Bay and Carpinteria Slough. We combined these samples with existing datasets from Seal Beach and Tijuana to form an 89-sample regional modern training set. Unconstrained cluster analysis divided the foraminiferal assemblages into four elevation-dependent faunal zones. Elevation exerts a major control over species distributions, explaining 16% of the variance in the dataset, and species are unimodally distributed along the elevation gradient. Consequently, we developed transfer functions to explore the potential for the use of the training set for quantifying past changes in marsh surface elevation. Our chosen model displays a strong relationship between observed and predicted marsh elevations in the modern data

set. With prediction uncertainties equivalent to  $\pm 0.18$  m at Mission Bay, the transfer function provides precise reconstructions of paleo-marsh surface elevation from appropriate fossil foraminiferal assemblages.

We perform an initial test of the applicability of the training set and associated transfer function by investigating fossil foraminifera preserved in sediment successions from the Mission Bay site. Here, hand-driven cores map the marsh stratigraphy and have the potential to provide evidence for late Holocene paleoenvironmental changes. The modern training set provides close analogues for the majority of fossil foraminiferal samples; however, many fossil samples contain *Arenoparrella mexicana*, a species not found in the modern samples. This disparity may reflect the infaunal living position of the species, which is not captured by the modern sampling approach. The Mission Bay site is not ideally suited to long-term relative sea-level reconstruction due to substantial anthropogenic modification and potential but unknown changes in tidal range over time. Instead, we limit our focus to three notable stratigraphic changes within the salt-marsh sediments. The abrupt and widespread change in stratigraphy, increase in low marsh taxa and quantitative reconstructions indicating decimeter-scale submergence may point towards the oldest change being associated with lateral spreading of the water-saturated sediments due to strong ground shaking from a local earthquake. Bayesian age-depth modeling indicates that this event might be contemporaneous with a moderate to large-magnitude earthquake that occurred on the Rose Canyon fault in the early to mid-18<sup>th</sup> century CE; however, further dating is required to more precisely constrain the age of the sedimentary evidence. Two younger stratigraphic changes are not consistent with this mechanism. A gradual increase in low marsh taxa in the mid 19<sup>th</sup> to early 20<sup>th</sup> century may relate to rerouting of the San Diego River into Mission Bay and resulting changes in sediment infilling and tidal range, while a faunabarren sand deposit encountered towards the landward edge of the marsh may reflect fluvial flooding.

The results presented here indicate the potential for our new foraminifera-based transfer function to support studies of the palaeoenvironmental evolution of the Southern Californian coastline. While the interpretation of the Mission Bay sequence remains preliminary due to the complexity of the site and the potential for unrecognized changes in tidal range, it appears likely that coastal sediments in this region may preserve evidence for the environmental effects of large earthquakes. Recognizing geological evidence for these events is potentially of considerable value for informing future hazard assessment and mitigation strategies in the densely populated Southern California. Future coastal studies should therefore seek to provide improved constraints on the magnitude and frequency of earthquakes in this region.

## ACKNOWLEDGMENTS

This study was supported by the US Department of Interior establishing grant #Y561461:03 for the Southwest Climate Science and by the Southern California Earthquake Center (Contribution No. 11012). SCEC is funded by NSF Cooperative Agreement EAR-1600087 & USGS Coopera-

tive Agreement G17AC00047. We gratefully acknowledge the Kendall-Frost Mission Bay Marsh Reserve and Isabelle Kay the Manager and Academic Coordinator of the Natural Reserve System UC San Diego for site access, helpful suggestions. Thanks are due to Matthew E. Kirby (Cal-State Fullerton) for the granulometric analysis and Pamela Buzas-Stephens and Martin A. Buzas for help with foraminiferal analysis in Carpinteria Slough. Matt Zebrowski of the Cartography Laboratory of the Department of Geography and Noah Bodzin of the Nanoelectronics Research Facility Department at UCLA (University of California Los Angeles), are thanked for the graphics and the SEM, respectively. Appendices 3–5 can be found linked to the online version of this article.

## REFERENCES

- Atwater, B.F., and Hemphill-Haley, E., 1997, Recurrence intervals for great earthquakes of the past 3500 years at northeastern Willapa Bay, Washington. In: U.S. Geological Survey Professional Paper, 1576, 108 pp.
- Avnaim-Katav, S., Milker, Y., Schmiedl, G., Sivan, D., Hyams-Kaphzan, O., Sandler, A., and Almogi-Labin, A., 2016, Impact of eustatic and tectonic processes on the southeastern Mediterranean shelf: Quantitative reconstructions using a foraminiferal transfer function: *Marine Geology*, v. 376, p. 26–38.
- Aquino-López, M. A., Blaauw, M., Christen, J. A., and Sanderson, N. K., 2018, Bayesian Analysis of 210Pb Dating: *Journal of Agricultural, Biological and Environmental Statistics*, v. 23, p. 317–333.
- Aquino-López, M.A., Ruiz-Fernández, A.C., Blaauw, M., and Sanchez-Cabeza, J.A., 2020, Comparing classical and Bayesian 210Pb dating models in human-impacted aquatic environments: *Quaternary Geochronology* 60, 101106.
- Avnaim-Katav, S., Gehrels, W.R., Brown, L., Fard, E., and MacDonald, M.G., 2017, Distributions of salt-marsh foraminifera along the coast of SW California, USA: implications for sea-level reconstructions: *Marine Micropaleontology*, v. 131, p. 25–43.
- Aydan, O., Ulusay, R. and Atak, V. O., 2008, Evaluation of Ground Deformations Induced by the 1999 Kocaeli Earthquake (Turkey) at Selected Sites on Shorelines: *Environmental Geology*, v. 54, p. 165–182.
- Barbosa, C. F., Scott, D. B., Seoane, J. C. S., and Turcq, B. J., 2005, Foraminiferal zonation as base lines for quaternary sea-level fluctuations in south-southeast Brazilian mangroves and marshes: *Journal of Foraminiferal Research*, v. 35, p. 22–43.
- Barnett, R. L., Garneau, M., and Bernatchez, P., 2016, Salt-marsh sea-level indicators and transfer function development for the Magdalen Islands in the Gulf of St. Lawrence, Canada: *Marine Micropaleontology*, v. 122, p. 13–26.
- Barlow, N. L., Shennan, I., Long, A. J., Gehrels, W. R., Saher, M. H., Woodroffe, S. A., and Hillier, C., 2013, Salt marshes as late Holocene tide gauges: *Global and Planetary Change*, v. 106, p. 90–110.
- Berkeley, A., Perry, C. T., Smithers, S. G., and Horton, B. P., 2008, The spatial and vertical distribution of living (stained) benthic foraminifera from a tropical, intertidal environment, north Queensland, Australia: *Marine Micropaleontology*, v. 69, p. 240–261.
- Bernhard, J. M., Ostermann, D. R., Williams, D. S., and Blanks, J. K., 2006, Comparison of two methods to identify live benthic foraminifera: A test between Rose Bengal and CellTracker Green with implications for stable isotope paleoreconstructions: *Paleoceanography and Paleoclimatology*, v. 21, p. 1–8.
- Birks, H. J. B., 1998, DG Frey and ES Deevey Review I: Numerical tools in palaeolimnology—Progress, potentialities, and problems: *Journal of Paleolimnology*, v. 20, p. 307–332.
- Blaauw, M., Christen, J. A., Aquino-Lopez, M. A., Esquivel-Vazquez, J., Gonzalez, O. M., Belding, T., Theiler, J., Gough B., and Karney, C., 2022, R package rplum version 0.2.2 (<https://cran.r-project.org/web/packages/rplum/index.html>).
- Brader, M., Garrett, E., Melnick, D. and Shennan, I., 2021, Sensitivity of tidal marshes as recorders of major megathrust earthquakes: constraints from the 25 December 2016 Mw 7.6 Chiloé earthquake, Chile: *Journal of Quaternary Science* 36, 991–1002. <https://doi.org/10.1002/jqs.3323>
- Callard, S. L., Gehrels, W. R., Morrison, B. V., and Grenfell, H. R., 2011, Suitability of salt-marsh foraminifera as proxy indicators of sea level in Tasmania: *Marine Micropaleontology*, v. 79, p. 121–131.
- Clarke, K. R., and Gorley, R. N., 2006, PRIMER v6: User Manual/Tutorial (Plymouth Routines in Multivariate Ecological Research): PRIMER-E, Plymouth, 190 p.
- Culver, S. J., and Horton, B. P., 2005, Infaunal marsh foraminifera from the outer banks, North Carolina, USA: *Journal of Foraminiferal Research*, v. 35, p. 148–170.
- de Rijk, S., and Troelstra, S. R., 1997, Salt marsh foraminifera from the Great Marshes, Massachusetts: environmental controls: *Palaeogeography, Palaeoclimatology, Palaeoecology*, v. 130, p. 81–112.
- Darienzo, M.E., and Peterson, C.D., 1995, Magnitude and frequency of subduction-zone earthquakes along the northern Oregon coast in the past 3000 years: *Oregon Geology*, 57, 3–12.
- Drexler, J. Z., Fuller, C. C., and Archfield, S., 2018, The approaching obsolescence of 137Cs dating of wetland soils in North America: *Quaternary Science Reviews*, v. 199, p. 83–96.
- Edwards, R. J., Wright, A. J., and van de Plassche, O., 2004, Surface distributions of salt-marsh foraminifera from Connecticut, USA: Modern analogues for high-resolution sea level studies: *Marine Micropaleontology*, v. 51, p. 1–21.
- Engelhart, S. E., Horton, B. P., Vane, C. H., Nelson, A. R., Witter, R. C., Brody, S. R., and Hawkes, A. D., 2013, Modern foraminifera,  $\delta^{13}C$ , and bulk geochemistry of central Oregon tidal marshes and their application in paleoseismology: *Palaeogeography, Palaeoclimatology, Palaeoecology*, v. 377, p. 13–27.
- Figueira, B. O., Grenfell, H., Hayward, B. W., and Alfaro, A. C., 2012, Comparison of rose bengal and celltracker green staining for identification of live salt-marsh foraminifera: *Journal of Foraminiferal Research*, v. 42, p. 206–215.
- Gehrels, W. R., 1994, Determining relative sea-level change from salt-marsh foraminifera and plant zones on the coast of Maine, USA: *Journal of Coastal Research*, 10, 990–1009.
- Gehrels, W. R., 1999, Middle and late Holocene sea-level changes in eastern Maine reconstructed from foraminiferal saltmarsh stratigraphy and AMS 14 C dates on basal peat: *Quaternary Research*, v. 52, p. 350–359.
- Gehrels, W. R., and van de Plassche, O., 1999, The use of *Jadammina macrescens* (Brady) and *Balticammina pseudomacrescens* Brönnimann, Lutze and Whittaker (Protozoa: Foraminiferida) as sea-level indicators: *Palaeogeography, Palaeoclimatology, Palaeoecology*, v. 149, p. 89–101.
- Gehrels, W. R., Milne, G. A., Kirby, J. R., Patterson, R. T., and Belknap, D. F., 2004, Late Holocene sea-level changes and isostatic crustal movements in Atlantic Canada: *Quaternary International*, v. 120, p. 79–89.
- Gehrels, W. R., Roe, H. M., and Charman, D. J., 2001, Foraminifera, testate amoebae and diatoms as sea-level indicators in UK salt-marshes: A quantitative multiproxy approach: *Journal of Quaternary Science*, v. 16, p. 201–220.
- Goldstein, S. T., and Harben, E. B., 1993, Taphofacies implications of infaunal foraminiferal assemblages in a Georgia salt marsh, Sapelo Island: *Micropaleontology*, v. 39, p. 53–62.
- Grant, L. B., and Rockwell, T. K., 2002, A northward-propagating earthquake sequence in coastal southern California: *Seismological Research Letters*, v. 73, p. 461–469.
- Guilbault, J. P., Clague, J. J., and Lapointe, M., 1996, Foraminiferal evidence for the amount of coseismic subsidence during a late Holocene earthquake on Vancouver Island, west coast of Canada: *Quaternary Science Reviews*, v. 15, p. 913–937.
- Foster, I. D. L., Mighall, T. M., Proffitt, H., Walling, D. E., and Owens, P. N., 2006, Post-depositional 137Cs mobility in the sediments of three shallow coastal lagoons, SW England: *Journal of Paleolimnology*, v. 35, p. 881–895.
- Hawkes, A. D., Horton, B. P., Nelson, A. R., and Hill, D. F., 2010, The application of intertidal foraminifera to reconstruct coastal subsi-

- dence during the giant Cascadia earthquake of AD 1700 in Oregon, USA: *Quaternary International*, v. 221, p. 116–140.
- Hayward, B. W., Le Coze, F., Vachard, D., and Gross, O., 2022, World Foraminifera Database: Accessed at <https://www.marinespecies.org/foraminifera> on 2022-08-19, DOI: 10.14284/305.
- Hippensteel, S. P., Martin, R. E., Nikitina, D., and Pizzuto, J. E., 2002, Interannual variation of marsh foraminiferal assemblages (Bombay Hook National Wildlife Refuge, Smyrna, DE): Do foraminiferal assemblages have a memory?: *Journal of Foraminiferal Research*, v. 32, p. 97–109.
- Hocking, E.P., Garrett, E., and Cisternas, M., 2017, Modern diatom assemblages from Chilean tidal marshes and their application for quantifying deformation during past great earthquakes: *Journal of Quaternary Science* 32, 396–415. doi:10.1002/jqs.2933
- Horton, B. P., Edwards, R. J., and Lloyd, J. M., 1999, A foraminiferal-based transfer function: Implications for sea-level studies: *Journal of Foraminiferal Research*, v. 29, p. 117–129.
- Horton, B. P., and Edwards, R. J., 2005, The application of local and regional transfer functions to the reconstruction of Holocene sea levels, north Norfolk, England: *The Holocene*, 15(2), 216–228.
- Horton, B. P., and Edwards, R. J., 2006, Quantifying Holocene sea level change using intertidal foraminifera: Lessons from the British Isles: *Cushman Foundation for Foraminiferal Research Special Publication*, v. 40, 97 p.
- Jeter, H. W., 2000, Determining the ages of recent sediments using measurements of trace radioactivity: *Terra Aqua*, v. 78, p. 21–28.
- Juggins, S., 2011, C2 Data Analysis Version 1.7.2: University of Newcastle, Newcastle upon Tyne.
- Juggins, S., and Birks, H. J. B., 2012, Quantitative environmental reconstructions from biological data, *in* Birks, H. J. B., et al. (eds.), *Tracking Environmental Change Using Lake Sediments*: Springer, Dordrecht, The Netherlands, p. 431–494.
- Kemp, A. C., Horton, B. P., and Culver, S. J., 2009, Distribution of modern salt-marsh foraminifera in the Albemarle–Pamlico estuarine system of North Carolina, USA: implications for sea-level research: *Marine Micropaleontology*, 72(3), 222–238.
- Kemp, A. C., Horton, B. P., Donnelly, J. P., Mann, M. E., Vermeer, M., and Rahmstorf, S., 2011, Climate related sea-level variations over the past two millennia: Proceedings of the National Academy of Sciences, v. 108, p. 11017–11022.
- Kemp, A. C., and Telford, R. J., 2015, *Transfer Functions: Handbook of Sea-Level Research*: John Wiley and Sons, Chichester, 470–499.
- Kemp, A. C., Wright, A. J., and Cahill, N., 2020, Enough is Enough, or More is More? Testing the Influence of Foraminiferal Count Size on Reconstructions of Paleo-Marsh Elevation: *Journal of Foraminiferal Research*, v. 50, p. 266–278.
- Legendre, P., and Fortin, M. J., 1989, Spatial pattern and ecological analysis: *Vegetatio*, v. 80, p. 107–138.
- Leorri, E., Gehrels, W. R., Horton, B. P., Fatela, F., and Cearreta, A., 2010, Distribution of foraminifera in salt marshes along the Atlantic coast of SW Europe: Tools to reconstruct past sea-level variations: *Quaternary International*, v. 221, p. 104–115.
- Lepš, J., and Šmilauer, P., 2003, *Multivariate Analysis of Ecological Data Using CANOCO*: Cambridge University Press, Cambridge, 269 p.
- Lienkaemper, J. J., and Bronk-Ramsey, C., 2009, OxCal: Versatile tool for developing paleoearthquake chronologies—a primer: *Seismological Research Letters*, v. 80, p. 431–434, DOI: 10.1785/gssrl.80.3.431.
- Lindvall, S., and Rockwell, T. K., 1995, Holocene activity of the Rose Canyon fault zone in San Diego, California: *Journal of Geophysical Research*, v. 100, B12, 24121–24132.
- Marcus, L., 1989, *The coastal wetlands of San Diego County*: State Coastal Conservancy, California, 64 p.
- Milker, Y., Horton, B. P., Nelson, A. R., Engelhart, S. E., and Witter, R. C., 2015, Variability of intertidal foraminiferal assemblages in a salt marsh, Oregon, USA: *Marine Micropaleontology*, v. 118, p. 1–16.
- Nelson, A. R., Sawai, Y., Jennings, A. E., Bradley, L. A., Gerson, L., Sherrod, B. L., Sabeany, J., and Horton, B. P., 2008, Great-earthquake paleogeodesy and tsunamis of the past 2000 years at Alsea Bay, central Oregon coast, USA: *Quaternary Science Reviews*, v. 27, p. 747–768.
- Nelson, A. R., Shennan, I., and Long, A. J., 1996, Identifying coseismic subsidence in tidal-wetland stratigraphic sequences at the Cascadia subduction zone of western North America: *Journal of Geophysical Research*, v. 101, p. 6115–6135.
- NOAA (2022) TWC0413 Quivira Basin, Mission Bay. Accessed at <https://tidesandcurrents.noaa.gov/stationhome.html?id=TWC0413> on 2022-08-19.
- Overpeck, J. T., Webb, T., III, and Prentice, I. C., 1985, Quantitative interpretation of fossil pollen spectra: Dissimilarity coefficients and the method of modern analogs: *Quaternary Research*, v. 23, p. 87–108.
- Patterson, R. T., 1990, Intertidal benthic foraminiferal biofacies on the Fraser River Delta, British Columbia: Modern distribution and paleoecological importance: *Micropaleontology*, v. 36, p. 183–199.
- Patterson, R. T., Gehrels, W. R., Belknap, D. F., and Dalby, A. P., 2004, The distribution of salt marsh foraminifera at Little Dipper Harbour New Brunswick, Canada: Implications for development of widely applicable transfer functions in sea-level research: *Quaternary International*, v. 120, p. 185–194.
- Phleger, F. B., and Bradshaw, J. S., 1966, Sedimentary environments in marine marshes: *Science*, v. 154, p. 155–153.
- Poland, J. F. and Piper, A. M., 1956, *Ground-water Geology of the Coastal Zone Long Beach-Santa Ana area, California*: U.S. Geological Survey Water-Supply Paper 1109.
- R Core Team, 2013, R: A language and environment for statistical computing: R Foundation for Statistical Computing, Vienna, Austria. Accessed at <http://www.R-project.org/>.
- Reimer, P. J., Austin, W. E. N., Bard, E., Bayliss, A., Blackwell, P. G., Bronk Ramsey, C., Butzin, M., Cheng, H., Edwards, R. L., Friedrich, M., Grootes, P. M., Guilderson, T. P., Hajdas, I., Heaton, T. J., Hogg, A. G., Hughen, K. A., Kromer, B., Manning, S. W., Muscheler, R., Palmer, J. G., Pearson, C., van der Plicht, J., Reimer, R. W., Richards, D. A., Scott, E. M., Southon, J. R., Turney, C. S. M., Wacker, L., Adolphi, F., Büntgen, U., Capano, M., Fahrni, S. M., Fogtmann-Schulz, A., Friedrich, R., Köhler, P., Kudsk, S., Miyake, F., Olsen, J., Reinig, F., Sakamoto, M., Sookdeo, A., and Talamo, S., 2020, The IntCal20 Northern Hemisphere Radiocarbon Age Calibration Curve (0–55 cal kBP): *Radiocarbon*, v. 62, p. 725–757.
- Reynolds, L. C., Simms, A. R., Ejarque, A., King, B., Anderson, R. S., Carlin, J. A., Bentz, J. M., Rockwell, T. K., and Peters, R., 2018, Coastal flooding and the 1861–1862 California storm season: *Marine Geology*, v. 400, p. 49–59.
- Rockwell, T. K., 2010, The Rose Canyon fault zone in San Diego: Fifth International Conference on Recent Advances in Geotechnical Earthquake Engineering and Soil Dynamics and Symposium in Honor of Professor I.M. Idriss, no. 7.06c, p. 1–9.
- Sadro, S., Gastil-Buhl, M., and Melack, J., 2007, Characterizing patterns of plant distribution in a southern California salt marsh using remotely sensed topographic and hyperspectral data and local tidal fluctuations: *Remote Sensing of Environment*, v. 110, p. 226–239.
- Sahakian, V., Bormann, J., Driscoll, N., Harding, A., Kent, G., and Wesnousky, S., 2017, Seismic constraints on the architecture of the Newport–Inglewood/Rose Canyon fault: Implications for the length and magnitude of future earthquake ruptures: *Journal of Geophysical Research*, v. 122, p. 2085–2105, DOI: 10.1002/2016JB013467.
- Sawai, Y., Horton, B. P., and Nagumo, T., 2004, The development of a diatom-based transfer function along the Pacific coast of eastern Hokkaido, northern Japan—an aid in paleoseismic studies of the Kuril subduction zone: *Quaternary Science Reviews*, v. 23, p. 23–24.
- Schelske, C. L., Peplow, A., Brenner, M., and Spencer, C. N., 1994, Low-background gamma counting: Applications for <sup>210</sup>Pb dating of sediments: *Journal of Paleolimnology*, v. 10, p. 115–128, DOI: 10.1007/BF00682508.
- Schönfeld, J., Alve, E., Geslin, E., Jorissen, F., Korsun, S., and Spezzaferri, S., 2012, The FOBIMO (FOraminiferal BIo-MONitoring) initiative—Towards a standardised protocol for soft-bottom benthic foraminiferal monitoring studies: *Marine Micropaleontology*, v. 94, p. 1–13.
- Scott, D. B., 1976, Brackish-water foraminifera from southern California and description of *Polysaccamina ipohalina* n. gen., n. sp.: *Journal of Foraminiferal Research*, v. 6, p. 312–321.

- Scott, D. B., Medioli, F. S., and Duffett, T. E., 1984, Holocene rise of relative sea level at Sable Island, Nova Scotia, Canada: *Geology*, 12(3), 173–176.
- Scott, D. B., and Medioli, F. S., 1980, Quantitative studies of marsh foraminiferal distributions in Nova Scotia; implications for sea level studies: Cushman Foundation for Foraminiferal Research, Special Publications, v. 17.
- Scott, D. B., and Hermelin, J. O. R., 1993, A device for precision splitting of micropaleontological samples in liquid suspension: *Journal of Paleontology*, v. 67, p. 151–154.
- Scott, D. B., Mudie, P. J., and Bradshaw, J. S., 2011, Coastal evolution of Southern California as interpreted from benthic foraminifera, ostracodes, and pollen: *Journal of Foraminiferal Research*, v. 41, p. 285–307.
- Shennan, I., Long, A. J., Rutherford, M. M., Green, F. M., Innes, J. B., Lloyd, J. M., Zong, Y., Walker, and K. J., 1996, Tidal marsh stratigraphy, sea-level change and large earthquakes, I: A 5000 year record in Washington, USA: *Quaternary Science Reviews* v. 15, p. 1023–1059.
- Shennan, I., Barlow N., Carver, G. A., Davies, F., Garrett, E., and Hocking, E., 2014, Great tsunamigenic earthquakes during the past 1000 yr on the Alaska megathrust: *Geology*, v. 42, p. 687–690.
- Shennan, I., Garrett, E., and Barlow N., 2016, Detection limits of tidal-wetland sequences to identify variable rupture modes of megathrust earthquakes: *Quaternary Science Reviews* v. 150, p. 1–30.
- Singleton, D. M., Rockwell, T. K., Murbach, D., Murbach, M., Maloney, J. M., Freeman, T., and Levy, Y., 2019, Late-Holocene Rupture History of the Rose Canyon Fault in Old Town, San Diego: Implications for Cascading Earthquakes on the Newport–Inglewood–Rose Canyon Fault System: *Bulletin of the Seismological Society of America*, v. 109, p. 855–874, DOI: 10.1785/0120180236.
- Southall, K. E., Gehrels, W. R., and Hayward, B. W., 2006, Foraminifera in a New Zealand salt marsh and their suitability as sea-level indicators: *Marine Micropaleontology*, v. 60, p. 167–179.
- Telford, R. J., and Birks, H. J. B., 2009, Evaluation of transfer functions in spatially structured environments: *Quaternary Science Reviews*, v. 28, p. 1309–1316.
- ter Braak, C. J., 1986, Canonical Correspondence Analysis: A new eigenvector technique for multivariate direct gradient analysis: *Ecology*, v. 67, p. 1167–1179.
- ter Braak, C. J., 1987, Unimodal models to relate species to environment: Wageningen University and Research, Pudoc, Wageningen, Netherlands, 152 p.
- ter Braak, C. J., and Juggins, S., 1993, Weighted averaging partial least squares regression (WA-PLS): An improved method for reconstructing environmental variables from species assemblages: *Hydrobiologia*, v. 269, p. 485–502.
- ter Braak, C. J., and Šmilauer, P., 2002, CANOCO reference manual and CanoDraw for Windows user's guide: Software for canonical community ordination (version 4.5).
- Watcham, E. P., Shennan, I., and Barlow, N. L. M., 2013, Scale considerations in using diatoms as indicators of sea level change: Lessons from Alaska: *Journal of Quaternary Science*, v. 28, p. 165–179.
- Williams, S., Garrett, E., Moss, P. T., Bartlett, R. E., and Gehrels, W. R., 2021, Development of a regional training set of contemporary salt-marsh foraminifera for Late Holocene sea-level reconstructions in southeastern Australia: *Open Quaternary*, v. 7, p. 1–29.
- Woodroffe, S. A., 2009, Recognising subtidal foraminiferal assemblages: Implications for quantitative sea-level reconstructions using a foraminifera-based transfer function: *Journal of Quaternary Science*, v. 24, p. 215–223.
- Woodroffe, S. A., and Horton, B. P., 2005, Holocene sea-level changes in the Indo-Pacific: *Journal of Asian Earth Sciences*, v. 25, p. 29–43.
- Wright, A. J., Edwards, R. J., and van de Plassche, O., 2011, Reassessing transfer-function performance in sea-level reconstruction based on benthic salt-marsh foraminifera from the Atlantic coast of NE North America: *Marine Micropaleontology*, v. 81, p. 43–62.
- Zedler, J. B., 1977, Salt marsh community structure in the Tijuana Estuary, California: *Estuarine and Coastal Marine Science*, v. 5, p. 39–53, DOI:10.1016/0302-3524(77)90072-X.
- Zedler, J. B., 1982, The ecology of southern California coastal salt marshes: A community profile: U.S. Fish and Wildlife Service, Biological Services Program, Washington, D. C. FWS/OBS 31/54, 110 p.
- Zedler, J. B., 2010, How frequent storms affect wetland vegetation: A preview of climate-change impacts: *Frontiers in Ecology and the Environment*, v. 8, p. 540–547, DOI: 10.1890/090109.
- Zedler, J. B., Covin, J., Nordby, C., Williams, P., and Boland, J., 1986, Catastrophic events reveal the dynamic nature of salt-marsh vegetation in Southern California: *Estuaries*, v. 9, p. 75–80, DOI:10.1007/BF02689746.
- Bermudez, P.J., 1935: Foraminiferos de la costa norte de Cuba: *Memorias de la Sociedad Cubana de Historia Natural*, v. 9, p. 129–224.
- Edwards, R. J., Wright, A. J., and van de Plassche, O., 2004, Surface distribution of salt-marsh foraminifera from Connecticut, USA: Modern analogues for high-resolution sea level studies: *Marine Micropaleontology*, v. 51, p. 1–21.
- Gehrels, W. R., and van de Plassche, O., 1999, The use of *Jadammina macrescens* (Brady) and *Balticammina pseudomacrescens* Brönnimann, Lutze and Whittaker (Protozoa: Foraminiferida) as sea-level indicators: *Palaeogeography, Palaeoclimatology, Palaeoecology*, v. 149(1), p. 89–101.
- Hawkes, A. D., Horton, B. P., Nelson, A. R., and Hill, D. F., 2010, The application of intertidal foraminifera to reconstruct coastal subsidence during the giant Cascadia earthquake of AD 1700 in Oregon, USA: *Quaternary International*, v. 221(1), p. 116–140.
- Hayward, B. W., Grenfell, H. R., Reid, C. M., and Hayward, K. A., 1999, Recent New Zealand Shallow-Water Benthic Foraminifera: Taxonomy, Ecologic Distribution, Biogeography, and use in Palaeoenvironmental Assessments: Institute of Geological and Nuclear Sciences Monograph 21, Lower Hutt, New Zealand, 264 p.
- Horton, B. P., and Edwards, R. J., 2006, Quantifying Holocene sea level change using intertidal foraminifera: lessons from the British Isles: Cushman Foundation for Foraminiferal Research Special Publication 40.
- Kemp, A. C., Horton, B. P., Vann, D. R., Engelhart, S. E., Grand Pre, C. A., Vane, C. H., Nikitina, D., and Anisfeld, S. C., 2012, Quantitative vertical zonation of salt-marsh foraminifera for reconstructing former sea level; an example from New Jersey, USA: *Quaternary Science Reviews*, v. 54, p. 26–39.
- Kornfeld, M.M., 1931, Recent littoral foraminifera from Texas and Louisiana: Stanford University, Department of Geology Contributions 1, p. 77–101.
- Loeblich, A. R., and Tappan, H., 1988, Foraminiferal genera and their classification: Van Nostrand Reinhold Company, New York, 1694 p.
- Milker, Y., Horton, B. P., Nelson, A. R., Engelhart, S. E., and Witter, R. C., 2015, Variability of intertidal foraminiferal assemblages in a salt marsh, Oregon, USA: *Marine Micropaleontology*, v. 118, p. 1–16.
- Murray, J. W., 1979, British nearshore foraminiferids, in Kermack, D. M., and Barners, R. S. K., (eds), *Synopsis of the British Fauna (New Series) No 16*: Academic Press, London, 62 p.
- Murray, J. W., 2006, *Ecology and Applications of Benthic Foraminifera*: Cambridge University Press, Cambridge, 426 p.
- Saunders, J.B., 1958, Recent foraminifera of mangrove swamps and river estuaries and their fossil counterparts in Trinidad: *Micropaleontology*, v. 4, p. 79–92.
- Scott, D.B., and Medioli, F.S., 1976, Brackish-water foraminifera from southern California and description of *Polysaccammina ipohalina*, n. gen., n. sp.: *Journal of Foraminiferal Research*, v. 6, p. 312–321.
- Wright, A. J., Edwards, R. J., and van de Plassche, O., 2011, Reassessing transfer-function performance in sea-level reconstruction based on benthic salt-marsh foraminifera from the Atlantic coast of NE North America: *Marine Micropaleontology*, v. 81(1), p. 43–62.

Received 29 August 2022  
Accepted 19 December 2022

## APPENDIX

APPENDIX 1. Station locations and elevations of the surface samples collected at Mission Bay (denoted with the initials MB) and Carpinteria Slough (denoted with initials CS\_ES and CS\_BM).

Station	Elevation (m NAVD88)	Latitude	Longitude
MB1	1.97 ± 0.03	32.79571817	-117.2300469
MB2	1.79 ± 0.03	32.79556795	-117.2299898
MB3	1.72 ± 0.03	32.79544384	-117.229916
MB4	1.51 ± 0.03	32.79528798	-117.2297848
MB5	1.67 ± 0.02	32.79517818	-117.2297051
MB6	1.62 ± 0.03	32.79504529	-117.2296134
MB7	1.53 ± 0.03	32.79489175	-117.2295014
MB9	1.68 ± 0.03	32.79459769	-117.2291939
MB10	1.69 ± 0.03	32.79453274	-117.2290229
MB11	1.65 ± 0.04	32.79421521	-117.2289268
MB12	1.34 ± 0.03	32.79376023	-117.2286616
CS_ES_0000	1.402 ± 0.05	34.40202091	-119.5390087
CS_ES_0001	1.515 ± 0.05	34.40209829	-119.5389592
CS_ES_0002	1.238 ± 0.05	34.40239373	-119.5389093
CS_ES_0003	1.481 ± 0.05	34.40260074	-119.5388961
CS_ES_0004	1.487 ± 0.05	34.40285185	-119.538805
CS_ES_0006	1.406 ± 0.05	34.40297654	-119.5385484
CS_ES_0009	1.62 ± 0.05	34.40238616	-119.5384893
CS_ES_00011	1.444 ± 0.05	34.40203793	-119.5385022
CS_ES_00014	1.576 ± 0.05	34.40208239	-119.5381408
CS_ES_00017	1.21 ± 0.05	34.40257221	-119.5381379
CS_ES_00018	1.43 ± 0.05	34.40272898	-119.5380533
CS_ES_00019	1.341 ± 0.05	34.4028443	-119.5380044
CS_ES_00020	1.507 ± 0.05	34.40312539	-119.537861
CS_ES_00021	1.483 ± 0.05	34.40242702	-119.5378648
CS_ES_00022	1.189 ± 0.05	34.40238539	-119.5374663
CS_ES_00023	1.463 ± 0.05	34.40227664	-119.537004
CS_ES_00025	1.328 ± 0.05	34.40242188	-119.5374724
CS_BM_01	1.258 ± 0.05	34.40369468	-119.539166
CS_BM_02	1.173 ± 0.05	34.40381091	-119.5390965
CS_BM_03	1.192 ± 0.05	34.40391	-119.5390453
CS_BM_04	1.005 ± 0.05	34.40391383	-119.539041
CS_BM_05	1.291 ± 0.05	34.40397556	-119.538996
CS_BM_06	1.496 ± 0.05	34.40398826	-119.5389825
CS_BM_07	1.47 ± 0.05	34.40399309	-119.5389645
CS_BM_08	1.445 ± 0.05	34.40417564	-119.5388702
CS_BM_09	1.538 ± 0.05	34.40427722	-119.5388218
CS_BM_010	1.646 ± 0.05	34.40442542	-119.5387243
CS_BM_011	1.885 ± 0.05	34.4047732	-119.5387714
CS_BM_012	1.714 ± 0.05	34.40484414	-119.5387269

APPENDIX 2. Locations and elevations of the sediment cores collected at Mission Bay.

Station	Elevation (m NAVD88)	Latitude	Longitude
MB16-01	1.62 ± 0.03	32.7954489	-117.2294143
MB16-03	1.69 ± 0.03	32.7945327	-117.2290229
MB17-04	1.50 ± 0.11	32.79317019	-117.2309233
MB17-05	1.77 ± 0.03	32.793113	-117.2308632
MB17-06	0.78 ± 0.10	32.79308955	-117.2308292
MB17-07	1.01 ± 0.10	32.79309609	-117.2307201
MB17-08	0.97 ± 0.10	32.79306009	-117.2306433
MB17-09	0.94 ± 0.10	32.7930239	-117.2304069
MB17-13	0.86 ± 0.10	32.7929683	-117.2301936
MB17-12	0.98 ± 0.10	32.7929719	-117.2300514



Cushman  
Foundation for  
Foraminiferal  
Research

Est. 1950